J. Fluid Mech. (2007), *vol.* 575, *pp.* 187–219. © 2007 Cambridge University Press
doi:10.1017/S0022112006004071 Printed in the United Kingdom

Near-critical hydraulic flows in two-layer fluids

ALFRED KLUWICK[1], STEFAN SCHEICHL[1] AND EDWARD A. COX[2]

[1]Institute of Fluid Dynamics and Heat Transfer, Vienna University of Technology, A-1040 Vienna, Austria

[2]School of Mathematical Sciences, University College Dublin, Dublin, Ireland

(Received 2 May 2005 and in revised form 29 August 2006)

This paper deals with the propagation of nearly resonant gravity waves in two-layer flows over a bottom topography assuming that both fluids are incompressible and inviscid. Evolution equations are derived for weakly nonlinear surface-layer and internal-layer waves in the hydraulic limit of infinite wavelength. Special emphasis is placed on the flow regime where the quadratic nonlinear parameter associated with internal-layer waves is small or vanishes. For example, this is the case for all possible density ratios if the velocities in both layers are equal and if the interface height is close to one-half the total fluid-layer height. The waves then exhibit so-called mixed nonlinearity leading in turn to the formation of positive and negative hydraulic jumps. Considerations based on a model equation for the internal dissipative–dispersive structure of hydraulic jumps indicate that the admissibility of discontinuities in this regime depends strongly on the relative magnitudes of dispersion and dissipation. Surprisingly, these admissible hydraulic jumps may violate the wave-speed-ordering relationship which requires that the upstream wave speed does not exceed the propagation speed of the discontinuity. An important example is provided by the inviscid hydraulic jump, which has been known for some time, although its non-classical nature, in that it transmits rather than absorbs waves, has apparently not been recognized before.

1. Introduction

Quasi-one-dimensional gas-dynamic flows and hydraulic single-layer flows over a bottom topography represent two examples where the effects caused by the nonlinearity of the governing equations of fluid mechanics can be studied most easily. As a consequence, they are included in most standard textbooks. If considerations are limited to perfect gases, both types of flow share many common features and, in fact, in the limit of weak nonlinearity are equivalent from a mathematical point of view. In both applications one has to distinguish between subcritical and supercritical flow regimes, i.e. states where the flow velocity is smaller or larger than the signalling velocity. Also, solutions of steady as well as unsteady flows are found to contain regions of multivaluedness, in general, which have to be eliminated by the insertion of discontinuities into the flow quantities. These discontinuities representing shocks in gas-dynamic flows and hydraulic jumps in single-layer flows are not uniquely defined by the initial data and boundary conditions for the problem under consideration. Therefore, a central issue is the identification of physically acceptable weak solutions. This is achieved by invoking the second law of thermodynamics, which rules out the formation of negative jumps leading to a decrease in the pressure in gas-dynamic flows or a sudden reduction in the fluid-layer thickness in hydraulic flows.

https://doi.org/10.1017/S0022112006004071 Published online by Cambridge University Press

In a strict sense the equivalence between gas-dynamic and hydraulic flows is lost if discontinuities form. This is due to the fact that the application of the one-dimensional version of the governing equations is rigorously justified for the investigation of gas-dynamic shocks, while it yields an approximate description of hydraulic jumps only when the acceleration of the fluid in the vertical direction is neglected. Using the one-dimensional form of the governing equations substantially simplifies investigation of the internal dissipative structure of shocks which emerges if thermoviscous effects are accounted for. As a consequence, the Navier–Stokes structure of gas-dynamic shocks is now well understood. In contrast, no model exists at present that allows the incorporation of viscosity and acceleration parallel to the front into a refined self-consistent description of hydraulic jumps. This is true even for the most simple case of laminar flow, although the (interactive) mechanism which causes the departure of the flow from the unperturbed upstream state has been clarified (see Gajjar & Smith 1983; Bowles & Smith 1992). The resulting lack of information, however, is not expected to be crucial as far as the admissibility of discontinuities is concerned when we consider the hydraulic limit, i.e. when the streamwise extent of the dissipative profile associated with the hydraulic jump is small compared with a characteristic wavelength. In fact, in the related gas-dynamic problem the conclusions regarding jump conditions derived from the evolution of the shock-layer problem are found to be completely equivalent to the requirement of entropy increase across the shock.

The situation outlined so far changes drastically if more general situations are considered. This was recognized first in studies dealing with the dynamics of dense gases where the so-called fundamental derivative, which characterizes the variation of the convected sound speed with density, may change sign and assume negative values over a finite range of pressures and densities (Thompson 1971; Cramer & Kluwick 1984; Kluwick 2001). Consequently, both positive and negative shocks can form and coexist in such a fluid, which is then said to exhibit mixed nonlinearity. Furthermore, it is found that the second-law requirement for entropy increase across the shock is no longer sufficient to eliminate all shocks that violate the wave-speed-ordering relationship

$$v_{wb} > v_s > v_{wa}. \tag{1.1}$$

In general, these inequalities are considered to be necessary and sufficient conditions for admissible discontinuities. Here v_w and v_s denote, respectively, the wave speed and the shock speed while the subscripts b and a refer to states before (upstream of) and after (downstream of) the shock.

The relationship (1.1), now commonly referred to as the Lax criterion (e.g. Lax 1957), is plausible for various reasons. First, it implies that discontinuities are formed by converging rather than diverging wavefronts. This suggests that discontinuities violating (1.1) may not be able to propagate as stable shocks but will disintegrate into shocks of smaller intensity, satisfying (1.1), and continuous waves. Second, a shock violating (1.1) involves wavefronts propagating away from the discontinuity and, so it has been argued, violates the natural requirement that acceptable solutions must depend continuously on the initial and boundary values (e.g. Germain 1972). Despite the plausibility of (1.1), it is now recognized that satisfying these geometric inequalities neither always rules out inadmissible shocks nor always constitutes a necessary condition for admissibility. In the above-mentioned case of dense gases, investigations of the thermoviscous shock structure carried out by Cramer & Crickenberger (1991) and Kluwick (1993) show that the geometric admissibility criterion (1.1) (as well

https://doi.org/10.1017/S0022112006004071 Published online by Cambridge University Press

as the requirement of entropy increase) may not be sufficient to guarantee that discontinuities have such a shock structure. Moreover, some discontinuities having a thermoviscous inner structure may violate (1.1). Viewed in a general mathematical context, shock waves in dense gases provide an example of a scalar conservation law such as $\partial u/\partial t + \partial f(u)/\partial x = 0$ where the flux f is not convex so that $\partial^2 f/\partial u^2$ changes sign. Then (1.1) must be replaced by inequalities based on the convex hull of f (see for example Keyfitz 1995). This result can be formulated as the so-called Oleinik condition (see Oleinik 1959, 1964 and § 3 below). We mention in the context of two-layer fluid flows the recent papers by Jiang & Smith (2001*a*, *b*), in which they invoke a 'steepening hypothesis' as a mechanism for shock insertion. This is equivalent to the Lax condition. Consistently with this, the steady-state wave equation they derive in the weak-shock limit has a convex flux, and phenomena associated with mixed nonlinearity are excluded. In the finite-amplitude case, their prediction of finite-strength shocks, which occur on the boundary of applicability of their theory, is in agreement with a non-convex flux.

More recently it has been shown that admissible shocks can exist that violate even the (more general) Oleinik condition. An example of this arises in the context of particle suspensions, where the shock structure involves not only dissipative but also dispersive terms (see Kluwick, Cox & Scheichl 2000). Again the general mathematical framework involves shocks waves for non-convex flux functions, but now the shocks arise as limits of diffusive–dispersive approximations (see Jacobs, McKinney & Shearer 1995; Hayes & LeFloch 1997).

The phenomenon of mixed nonlinearity associated with a non-convex flux function has been encountered more recently also in two-layer flows over a topography, thus extending the analogy between one-dimensional gas-dynamic flows and hydraulic flows mentioned before. In such a system two types of waves have to be distinguished. The propagation speed of weakly nonlinear free-surface-layer waves is found to be a strictly monotonic function of the wave amplitude, resulting in flows analogous to classical gas-dynamics. In contrast, the propagation speed associated with small-amplitude finite-rate internal-layer waves is not monotonic. Investigations dealing with the hydraulic limit of infinite wavelength, therefore, will have to face problems similar to those occurring in the field of dense gas-dynamics. Apparently, flows of this type have not been studied systematically yet. This is one of the main aims of the present study, which is structured as follows.

Section 2 deals with the problem formulation and the derivation of evolution equations for weakly nonlinear surface-layer and internal-layer waves in two-layer flows over a topography. Specifically, it is assumed that the undisturbed state is close to a critical state for which one of the linear wave speeds vanishes. This, for example, is the case in situations where the velocities in both fluid layers, taken to be of almost the same thickness, are equal and results in a resonant wave response to topographic forcing. Here, special emphasis is placed on the case of internal-layer waves having the property that the quadratic nonlinearity is of the same size as the wave amplitude and may change sign.

Representative solutions of the evolution equation for internal-layer waves exhibiting mixed nonlinearity are presented in § 3. These include steady flows past single humps and results describing the unsteady transition between different possible steady states. Solutions which include hydraulic jumps are constructed on the basis of the Oleinik condition, which for the type of problems considered here is seen to be equivalent to the wave-speed-ordering principle (1.1) in the generalized sense that the equality signs have to be included.

https://doi.org/10.1017/S0022112006004071 Published online by Cambridge University Press

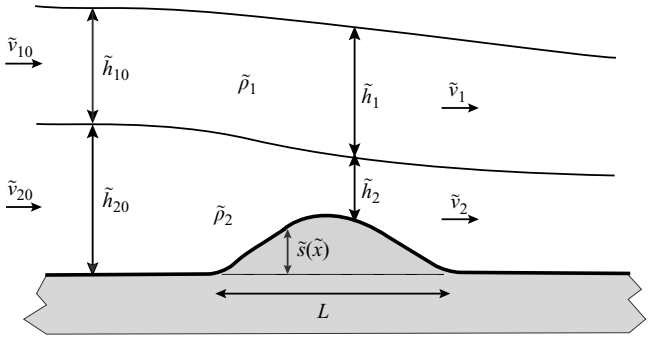


FIGURE 1. Problem and notation used for two-layer fluid flow over an isolated obstacle.

A rigorous investigation of this principle requires analysis of the internal dissipative dispersive structure of hydraulic jumps, which, unfortunately, is not known at present. Further comments on shock admissibility summarized in § 4, therefore, are based on a model equation which exhibits the correct dispersive behaviour but is only approximate as far as dissipative effects are concerned. Despite this obvious deficiency, this model equation is expected to provide at least a qualitative description of how possible shock profiles are affected by the relative magnitudes of dispersion and dissipation. Insight is further gained into how lossless hydraulic jumps emerge in the limit of vanishing dissipation, as predicted by existing theories of inviscid internal-layer waves of large but finite wavelength (e.g. Kakutani & Yamasaki 1978; Helfrich, Melville & Miles 1984; Melville & Helfrich 1987). Also discussed is the question of how these jumps can be incorporated in the strictly hyperbolic limit of infinite wavelength, where dispersion no longer enters the evolution equation.

2. Derivation of evolution equations

We investigate the propagation of weakly nonlinear gravity waves in a two-layer fluid over a bottom topography when the fluid is assumed to be inviscid and incompressible. The flow is contained within a two-dimensional channel, with an isolated obstacle located on what is otherwise a flat bottom. The problem and notation used are illustrated in figure 1.

2.1. *Formulation*

We consider a flow perturbed from a uniform state either by the instantaneous formation of an obstacle or by flow variations upstream or downstream of an existing obstacle. We assume that the obstacle is of characteristic length $\tilde{L}$ and height $\tilde{z}=\tilde{s}(\tilde{x})$ with maximum height small compared with its length. Specifically, we consider perturbations of a uniform flow having flow speeds $\tilde{v}_{10}$, $\tilde{v}_{20}$ and constant fluid depths $\tilde{h}_{10}$, $\tilde{h}_{20}$. The subscripts 1, 2 denote the surface and internal layers, respectively, and the fluid layers are distinguished by their densities $\tilde{\rho}_1$, $\tilde{\rho}_2$.

A natural non-dimensionalization of the governing equations involves the length $\tilde{L}$, the total depth $\tilde{h}_{10}+\tilde{h}_{20}$ and the phase velocity of surface gravity waves, $[\tilde{g}(\tilde{h}_{10}+\tilde{h}_{20})]^{1/2}$, as reference quantities. Non-dimensional variables are then defined by

$$\left.\begin{aligned} &\tilde{x}=\tilde{L}x, \quad \tilde{z}=(\tilde{h}_{10}+\tilde{h}_{20})z, \quad \tilde{s}=(\tilde{h}_{10}+\tilde{h}_{20})s, \quad \tilde{t}=\frac{\tilde{L}}{[\tilde{g}(\tilde{h}_{10}+\tilde{h}_{20})]^{1/2}}t,\\ &\tilde{h}_i=(\tilde{h}_{10}+\tilde{h}_{20})h_i, \quad \tilde{v}_i=[\tilde{g}(\tilde{h}_{10}+\tilde{h}_{20})]^{1/2}v_i, \quad \tilde{P}_i=\tilde{\rho}_i\tilde{g}(\tilde{h}_{10}+\tilde{h}_{20})P_i. \end{aligned}\right\} \tag{2.1}$$

https://doi.org/10.1017/S0022112006004071 Published online by Cambridge University Press

The depths, velocities and pressure in the two fluid layers, $i = 1, 2$, are denoted by $h_i(x, t)$, $v_i(x, t)$ and $P_i(x, z, t)$, with $\tilde{g}$ the gravitational acceleration.

Since the characteristic length $\tilde{L}$ is assumed to be large compared with the unperturbed heights, the flow in both layers is governed by the one-dimensional form of the Euler equations,

$$\frac{\partial v_i}{\partial t} + v_i \frac{\partial v_i}{\partial x} = -\frac{\partial P_i}{\partial x}, \tag{2.2}$$

$$\frac{\partial h_i}{\partial t} + \frac{\partial}{\partial x}(h_i v_i) = 0, \tag{2.3}$$

where $i = 1, 2$. Similarly to the case of single-layer flow (see for example Peregrine 1974), we assume a hydrostatic pressure distribution in each layer, so that

$$\left.\begin{aligned} P_1 &= P_a + (h_1 + h_2 + s - z), \\ P_2 &= \rho P_a + (\rho h_1 + h_2 + s - z), \end{aligned}\right\} \tag{2.4}$$

where $\rho = \tilde{\rho}_1/\tilde{\rho}_2$ and P_a denotes the pressure immediately above the top layer non-dimensionalized with respect to $\tilde{\rho}_1 \tilde{g}(\tilde{h}_{10} + \tilde{h}_{20})$. This form of simplification was used by Armi (1986), who considered steady two-layer flows through contractions and over sills, allowing for a perturbation level of order 1. The present study is more restrictive, in that it concentrates on small-amplitude disturbances of a uniform state but also more general in that it includes unsteady effects. Throughout the analysis we will assume $0 < \rho \leqslant 1$ for stability. Equations (2.2)–(2.4) can be formulated as

$$\frac{\partial \boldsymbol{u}}{\partial t} + \boldsymbol{A}(\boldsymbol{u})\frac{\partial \boldsymbol{u}}{\partial x} + \frac{\mathrm{d}s}{\mathrm{d}x}\boldsymbol{b} = \boldsymbol{0} \tag{2.5}$$

for the fluid flow $\boldsymbol{u} = (v_2, h_2, v_1, h_1)^T$, where

$$\boldsymbol{A}(\boldsymbol{u}) = \begin{pmatrix} v_2 & 1 & 0 & \rho \\ h_2 & v_2 & 0 & 0 \\ 0 & 1 & v_1 & 1 \\ 0 & 0 & h_1 & v_1 \end{pmatrix} \tag{2.6}$$

and

$$\boldsymbol{b} = (1, 0, 1, 0)^T. \tag{2.7}$$

The roots of the characteristic equation

$$\det(\boldsymbol{A}(\boldsymbol{u}) - \lambda \boldsymbol{I}) = [(v_1 - \lambda)^2 - h_1][(v_2 - \lambda)^2 - h_2] - \rho h_1 h_2 = 0 \tag{2.8}$$

identify the wave speeds $\lambda(\boldsymbol{u})$. With the roots ordered as $\lambda_1 \leqslant \lambda_2 \leqslant \lambda_3 \leqslant \lambda_4$, we can associate roots λ_2, λ_3 with wave propagation due to the inclusion of a lower fluid layer and λ_1, λ_4 with the surface-layer wave propagation. Of course, waves with speeds λ_2, λ_3 involve a distortion of the free surface as well; however, as they cannot occur in the case of a single-layer fluid, they are termed internal waves. A critical flow state $\boldsymbol{u}_c = (v_{2c}, h_{2c}, v_{1c}, h_{1c})^T$ is identified with the vanishing of one of the resulting wave speeds $\lambda = \lambda_j(\boldsymbol{u}_c)$. With an undisturbed state $\boldsymbol{u}_0 = (v_{20}, h_{20}, v_{10}h_{10})^T$ close to this critical flow, a wave generated at the obstacle will be trapped at the site of the obstacle, resulting in a resonant wave response to the obstacle-forcing, the details of which are now to be determined.

https://doi.org/10.1017/S0022112006004071 Published online by Cambridge University Press

2.2. Evolution equation for $\Gamma = O(1)$

The unperturbed conditions near criticality are chosen as

$$v_{i0} = v_{ic} + \bar{\sigma}, \quad h_{i0} = h_{ic}, \quad i = 1, 2, \tag{2.9}$$

where $\bar{\sigma} \ll 1$ is introduced as a velocity-detuning parameter. The standard expansion

$$\boldsymbol{u} = \boldsymbol{u}_0 + \epsilon \boldsymbol{u}^{(1)} + \epsilon^2 \boldsymbol{u}^{(2)} + O(\epsilon^3) \tag{2.10}$$

is assumed, with the scalings $x, \tau = \epsilon t$ for $\boldsymbol{u}^{(i)} = \boldsymbol{u}^{(i)}(x, \tau)$ describing disturbances of $O(\epsilon)$ trapped over the obstacle and evolving slowly in time. The perturbed fluid flow represents a resonant response of $O(\epsilon)$ generated by the $O(\epsilon^2)$ obstacle forcing

$$s = \epsilon^2 s_2(x). \tag{2.11}$$

We assume that $\bar{\sigma} = \epsilon\sigma$, ensuring that velocity detuning enters the describing equations at the same order as the nonlinear terms.

In component form equation (2.5) is

$$\epsilon \frac{\partial u_i}{\partial \tau} + A_{ij}(\boldsymbol{u}) \frac{\partial u_j}{\partial x} + \epsilon^2 \frac{\mathrm{d}s_2}{\mathrm{d}x} b_i = 0. \tag{2.12}$$

The speed matrix $\boldsymbol{A}(\boldsymbol{u})$ expanded about the critical state has elements of the form

$$A_{ij} = A_{ij}^{(0)} + \epsilon D_{ij} + B_{ijl}(u_l - u_{l_c}) + \cdots, \tag{2.13}$$

where

$$A_{ij}^{(0)} = A_{ij}(\boldsymbol{u}_c), \quad D_{ij} = \sigma \delta_{ij}, \quad B_{ijl} = \frac{\partial A_{ij}}{\partial u_l}(\boldsymbol{u}_c) \tag{2.14}$$

and δ_{ij} is the Kronecker delta. Equations (2.12)–(2.14) imply on equating coefficients of ϵ that

$$\text{at } O(\epsilon), \quad A_{ij}^{(0)} \frac{\partial u_j^{(1)}}{\partial x} = 0, \tag{2.15}$$

$$\text{at } O(\epsilon^2), \quad A_{ij}^{(0)} \frac{\partial u_j^{(2)}}{\partial x} = -\frac{\partial u_i^{(1)}}{\partial \tau} - \sigma \frac{\partial u_i^{(1)}}{\partial x} - B_{ijl} u_l^{(1)} \frac{\partial u_j^{(1)}}{\partial x} - \frac{\mathrm{d}s_2}{\mathrm{d}x} b_i. \tag{2.16}$$

If the generated flow over the obstacle is localized, non-trivial solutions to (2.15) are given by

$$u_j^{(1)} = U(x, \tau) r_j \tag{2.17}$$

where $A_{ij}^{(0)} r_j = 0$, providing that

$$\det \boldsymbol{A}^{(0)} = \left(v_{1c}^2 - h_{1c}\right)\left(v_{2c}^2 - h_{2c}\right) - \rho h_{1c} h_{2c} = 0. \tag{2.18}$$

We note in (2.18) that $h_{1c} + h_{2c} = h_{10} + h_{20} = 1$.

As one would expect, on comparing (2.8) and (2.18), the condition for constructing a disturbance generated at the obstacle and subsequently trapped over the obstacle is simply the requirement that the unperturbed flow satisfies the critical flow conditions $\lambda(\boldsymbol{u}_c) = 0$. A similar condition to (2.18) is found in Shen (1992), where it is observed that specifying the ratio v_{1c}/v_{2c} then enables the critical velocities to be determined for a given ρ and h_{1c}. From (2.18) we have the admissible inequalities, either

$$v_{1c}^2 \geqslant h_{1c}, \quad v_{2c}^2 \geqslant h_{2c}, \tag{2.19}$$

or

$$v_{1c}^2 \leqslant h_{1c}, \quad v_{2c}^2 \leqslant h_{2c}, \tag{2.20}$$

https://doi.org/10.1017/S0022112006004071 Published online by Cambridge University Press

(2.19) being associated with a resonant surface-layer wave and (2.20) with the internal-layer wave.

The scalar amplitude factor U in (2.17) can be determined by requiring the existence of non-trivial solutions for $\boldsymbol{u}^{(2)}$ at $O(\epsilon^2)$. The solvability condition at $O(\epsilon^2)$, namely that the right-hand side of (2.16) is orthogonal to $\boldsymbol{l}$, the left null vector of $A_{ij}^{(0)}$, generates the nonlinear evolution equation

$$\frac{\partial U}{\partial \tau} + \sigma \frac{\partial U}{\partial x} + \Gamma U \frac{\partial U}{\partial x} = -\beta \frac{\mathrm{d}s_2}{\mathrm{d}x}, \tag{2.21}$$

where

$$\Gamma = \frac{l_i B_{ijl} r_j r_l}{l_p r_p}, \quad \beta = \frac{l_i b_i}{l_p r_p} \tag{2.22}$$

and

$$l_m A_{mj}^{(0)} = 0. \tag{2.23}$$

Equation (2.21) includes the effect of wave distortion in the term multiplying Γ, obstacle-forcing in the β term, and off-resonant velocity detuning measured by σ.

The critical-speed matrix $\boldsymbol{A}(\boldsymbol{u}_c)$ determined by (2.6) has left and right null vectors

$$\left.\begin{aligned} \boldsymbol{l} &= \left(1, -\frac{v_{2c}}{h_{2c}}, -1 + \frac{v_{2c}^2}{h_{2c}}, \frac{1-\rho-v_{2c}^2/h_{2c}}{v_{1c}}\right)^T, \\ \boldsymbol{r} &= \left(h_{1c}(1-\rho) - v_{1c}^2, -h_{1c}v_{2c} + v_{2c}v_{1c}^2, -v_{1c}v_{2c}/h_{1c}v_{2c}\right)^T \end{aligned}\right\} \tag{2.24}$$

and the only nonzero components of B_{ijl} are

$$B_{111} = B_{212} = B_{221} = B_{333} = B_{434} = B_{443} = 1. \tag{2.25}$$

Using (2.24), (2.25) the nonlinear parameter Γ given by (2.22) is evaluated to be given by

$$\Gamma = \frac{3v_{2c}}{2h_{2c}} \left[\frac{v_{2c}^2\left(v_{1c}^2 - h_{1c}\right)^2 + v_{1c}^2\left(v_{2c}^2 - h_{2c}\right)h_{2c}}{v_{2c}\left(h_{1c} - v_{1c}^2\right) + v_{1c}\left(h_{2c} - v_{2c}^2\right)} \right], \tag{2.26}$$

the forcing parameter β being given by

$$\beta = \frac{v_{2c}}{2\left[v_{2c}\left(h_{1c} - v_{1c}^2\right) + v_{1c}\left(h_{2c} - v_{2c}^2\right)\right]}, \tag{2.27}$$

where v_{1c}, v_{2c} satisfy (2.18). It is clear from inequalities (2.19) and (2.20) that when $v_{1c} \geqslant 0$, $v_{2c} \geqslant 0$ the parameter β is negative for resonant surface-layer waves and positive for resonant internal waves.

The behaviour of the nonlinear parameter Γ given by (2.26) is more complicated. For resonant surface-layer waves inequality (2.19) is satisfied, and if in addition $v_{1c} > 0$, $v_{2c} > 0$ then $\Gamma \leqslant 0$ for all possible values of the density ratio and unperturbed fluid depths. In figure 2 the parameter $\Gamma(\rho, h_{1c})$ is plotted for values $v_{1c} = v_{2c} = v_c$ satisfying (2.18) and (2.19).

A particular limiting case is the single-layer fluid obtained on setting $\rho = 1$, $v_{1c} = v_{2c} = 1$. Then $\Gamma = -3/2$ and the total fluid depth $h = 1 + \epsilon h^{(1)} + O(\epsilon^2)$ is constructed from

$$\frac{\partial h^{(1)}}{\partial \tau} - \frac{3}{2} h^{(1)} \frac{\partial h^{(1)}}{\partial x} = \frac{1}{2} \frac{\mathrm{d}s_2}{\mathrm{d}x}. \tag{2.28}$$

With dispersion included, an equation similar to (2.28) was derived for a moving pressure disturbance by Akylas (1984) and for a fixed obstacle by Cole (1985). Implied

https://doi.org/10.1017/S0022112006004071 Published online by Cambridge University Press

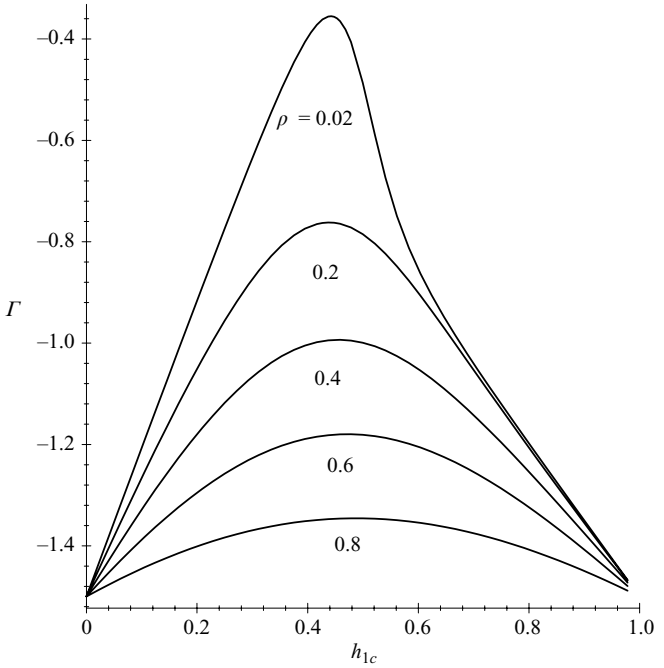


FIGURE 2. The nonlinear parameter Γ given by (2.26) for resonant surface waves, for various values of ρ (see (2.4)).

by (2.28) is a nonlinear distortion of the initial data, with positive portions of the wave distorted backwards and negative portions distorted forwards. This distortion eventually requires, within the hydrostatic approximation, the insertion of jump discontinuities into the flow. It is useful to recognize that U in (2.21) is proportional to the perturbed total fluid depth, and hence the only allowable jumps are those which lead to a sudden increase in the total depth of the fluid. The *qualitative* behaviour of resonant surface-layer waves will be similar to (2.28).

For conditions where the internal-layer wave is resonant, the wave behaviour can be distinctly different. For illustration, consider again the case where $v_{1c} = v_{2c} = v_c \geqslant 0$ satisfy (2.18), but now with values of $v_c(\rho, h_{1c})$ satisfying inequality (2.20). As shown in figure 3, $\Gamma(\rho, h_{1c})$ given by (2.26) can change sign depending on the particular critical conditions imposed. Clearly, if the unperturbed height h_{1c} of the upper fluid layer exceeds a certain value, which is dependent on the density ratio ρ but, interestingly, is always close to one-half, then the nonlinear parameter Γ becomes positive. This results through nonlinear wave evolution in the formation of negative hydraulic jumps, where a sudden decrease in the total layer thickness occurs. Such phenomena cannot occur in the case of a single-layer fluid described by (2.28) and are a feature of internal waves. For a given critical flow, (2.21) allows for either positive or negative hydraulic jumps but not their simultaneous formation.

Obviously, the asymptotic analysis which leads to (2.21) assumes that $\Gamma = O(1)$ and will break down in the vicinity of a transition point where the nonlinear parameter Γ vanishes. That such transition points occur can be seen from figure 4, where a curve is plotted, in the (v_c, h_{1c}) parameter space, along which Γ is identically zero. As mentioned before, the precise value of h_{1c} associated with $\Gamma = 0$ exhibits a weak dependence on the density ratio only and is always close to one-half. For values

https://doi.org/10.1017/S0022112006004071 Published online by Cambridge University Press

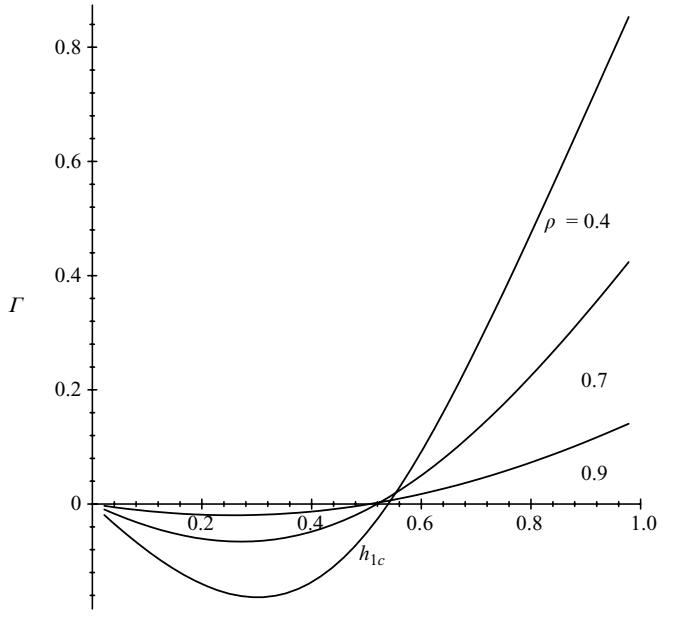


FIGURE 3. Γ given by (2.26) for resonant internal-layer waves, for various values of ρ.

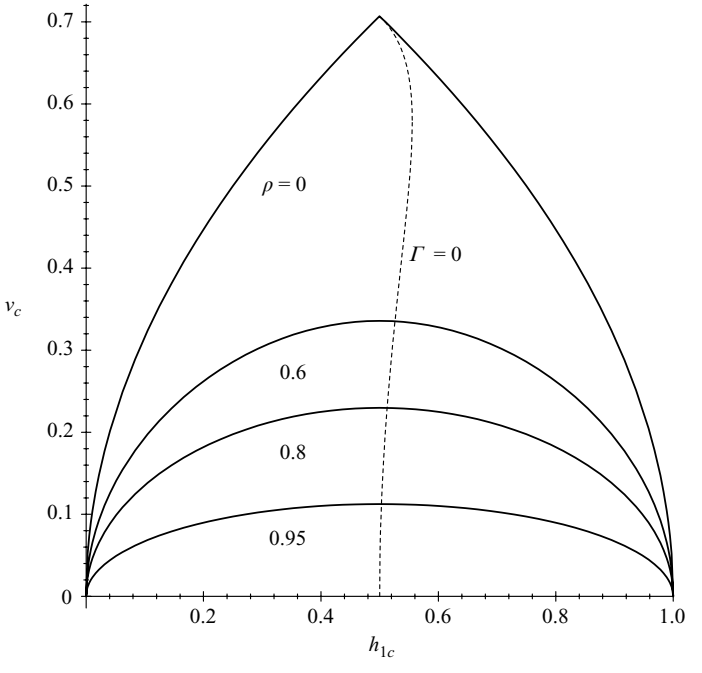


FIGURE 4. Transition curve along which the nonlinear coefficient Γ vanishes for resonant internal-layer waves.

of v_c and h_{1c} away from this curve the wave evolution will be described by (2.21) with either $\Gamma > 0$ or $\Gamma < 0$. However, within a $\Gamma = O(\epsilon)$ neighbourhood of this curve, small terms neglected in constructing (2.21) become of the same order as the included nonlinear correction term $\Gamma U U_x$ and a separate analysis is then required. Asymptotic

https://doi.org/10.1017/S0022112006004071 Published online by Cambridge University Press

expansions were developed by Cramer & Sen (1992) and Kluwick & Cox (1998) to include this $\Gamma = O(\epsilon)$ case for general quasi-linear systems of hyperbolic equations. These techniques will be applied here.

2.3. *Internal-layer waves: $\Gamma = O(\epsilon)$ case*

We consider expansions appropriate for internal-layer waves of perturbed amplitude $O(\epsilon)$ when the critical flow conditions imply that $\Gamma(v_{1c}, v_{2c}, h_{1c}, \rho) = O(\epsilon)$. Nonlinear effects will now become significant on the longer time scale $O(\epsilon^{-2})$. We assume that the height of the obstacle scales as $O(\epsilon^3)$ to generate a forcing term which enters at the same order as nonlinear effects. The velocity detuning of the upstream velocity from criticality will be significant now on an $O(\epsilon^2)$ scale. Hence, we choose

$$v_{io} = v_{ic} + \epsilon^2\sigma, \quad h_{io} = h_{ic}, \quad i = 1, 2, \tag{2.29}$$

and assume an expansion for $\boldsymbol{u} = (v_2, h_2, v_1, h_1)^T$ of the form

$$\boldsymbol{u} = \boldsymbol{u}_0 + \epsilon\boldsymbol{u}^{(1)} + \epsilon^2\boldsymbol{u}^{(2)} + O(\epsilon^3), \tag{2.30}$$

where each component $\boldsymbol{u}^{(j)}$ depends now on the resonant scalings x and $\tau = \epsilon^2 t$.

With the obstacle geometry $s = \epsilon^3 s_3(x)$, (2.5) in component form is now

$$\epsilon^2\frac{\partial u_i}{\partial \tau} + A_{ij}(\boldsymbol{u})\frac{\partial u_j}{\partial x} + \epsilon^3\frac{\mathrm{d}s_3}{\mathrm{d}x}b_i = 0. \tag{2.31}$$

The coefficient matrix A_{ij} is expanded as

$$A_{ij} = A_{ij}^{(0)} + B_{ijl}(u_l - u_{lc}) + \epsilon^2 D_{ij} + \cdots, \tag{2.32}$$

where

$$A_{ij}^{(0)} = A_{ij}(\boldsymbol{u}_c), \quad D_{ij} = \sigma\delta_{ij}, \quad B_{ijl} = \frac{\partial A_{ij}}{\partial u_l}(\boldsymbol{u}_c). \tag{2.33}$$

It is now assumed that B_{ijl} has the expansion

$$B_{ijl} = B_{0ijl} + \epsilon B_{1ijl} + O(\epsilon^2), \tag{2.34}$$

which enables a small, but non-zero, value for Γ to be accounted for. When expansions (2.30) for $\boldsymbol{u}$ and (2.32) for A_{ij} are substituted into (2.31) we have, again at $O(\epsilon)$,

$$u_j^{(1)} = U(x, \tau)r_j, \tag{2.35}$$

where $A_{ij}^{(0)}r_j = 0$ providing the components of $\boldsymbol{u}_c$ satisfy (2.18) and a localized disturbance is assumed. The quantities $u_j^{(2)}$ and $u_j^{(3)}$ satisfy the following:

$$\text{at } O(\epsilon^2), \quad A_{ij}^{(0)}\frac{\partial u_j^{(2)}}{\partial x} = -B_{0ijl}u_l^{(1)}\frac{\partial u_j^{(1)}}{\partial x}, \tag{2.36}$$

$$\text{at } O(\epsilon^3), \quad A_{ij}^{(0)}\frac{\partial u_j^{(3)}}{\partial x} = -\frac{\partial u_i^{(1)}}{\partial \tau} - \sigma\frac{\partial u_i^{(1)}}{\partial x} - B_{0ijl}\left(u_l^{(2)}\frac{\partial u_j^{(1)}}{\partial x} + u_l^{(1)}\frac{\partial u_j^{(2)}}{\partial x}\right) - B_{1ijl}u_l^{(1)}\frac{\partial u_j^{(1)}}{\partial x} - \frac{\mathrm{d}s_3}{\mathrm{d}x}b_i. \tag{2.37}$$

We now proceed as before. The solvability condition for $\boldsymbol{u}^{(2)}$, $\boldsymbol{u}^{(3)}$, namely that the right-hand sides of (2.36) and (2.37) are orthogonal to $\boldsymbol{l}$ (the left null vector of $A_{ij}^{(0)}$), gives for (2.36)

$$\frac{l_i B_{0ijl} r_j r_l}{l_p r_p} = 0. \tag{2.38}$$

On comparison with (2.22) this identifies a critical state where Γ is at most $O(\epsilon)$.

https://doi.org/10.1017/S0022112006004071 Published online by Cambridge University Press

An evolution equation for the amplitude function $U(x,\tau)$ is given by the solvability condition for $\boldsymbol{u}^{(3)}$ at $O(\epsilon^3)$:

$$l_i r_i \left(\frac{\partial U}{\partial \tau} + \sigma \frac{\partial U}{\partial x}\right) + l_i B_{0ijl} r_l \frac{\partial u_j^{(2)}}{\partial x} U + l_i B_{0ijl} r_j u_l^{(2)} \frac{\partial U}{\partial x} + l_i B_{1ijl} r_j r_l U \frac{\partial U}{\partial x} + l_i b_i \frac{\mathrm{d}s_3}{\mathrm{d}x} = 0. \tag{2.39}$$

As one would expect, the evolution equation (2.39) for $U(x,\tau)$ contains terms involving $\boldsymbol{u}^{(2)}$. The nature of these terms becomes clearer on introducing the vectors

$$b_j = l_i B_{0ijl} r_l, \quad c_l = l_i B_{0ijl} r_j \tag{2.40}$$

into (2.39) to give

$$l_i r_i \left(\frac{\partial U}{\partial \tau} + \sigma \frac{\partial U}{\partial x}\right) + \overbrace{b_j \frac{\partial u_j^{(2)}}{\partial x}}^{P} U + \overbrace{c_l u_l^{(2)}}^{Q} \frac{\partial U}{\partial x} + l_i B_{1ijl} r_j r_l U \frac{\partial U}{\partial x} + l_i b_i \frac{\mathrm{d}s_3}{\mathrm{d}x} = 0. \tag{2.41}$$

To evaluate the terms labelled P and Q in (2.41) we use the fact that the vectors $\boldsymbol{b}$ and $\boldsymbol{c}$ are orthogonal to $\boldsymbol{r}$ and employ the construction

$$b_j = \alpha_\lambda A_{\lambda j}^{(0)}, \quad c_l = \gamma_\mu A_{\mu l}^{(0)}, \tag{2.42}$$

where $A_{\lambda j}^{(0)}$, $A_{\mu j}^{(0)}$, $j = 1,\ldots,4$, denote the three linearly independent row vectors of $\boldsymbol{A}^{(0)}$; λ, μ take the three values corresponding to the independent rows of $\boldsymbol{A}^{(0)}$. Then P is determined from (2.36) as the weighted sum

$$b_j \frac{\partial u_j^{(2)}}{\partial x} = -\alpha_\lambda B_{0\lambda jl} r_j r_l U \frac{\partial U}{\partial x}. \tag{2.43}$$

Integration of (2.36) also leads to a weighted sum for Q:

$$c_l u_l^{(2)} = -\tfrac{1}{2}\gamma_\mu B_{0\mu lk} r_l r_k U^2, \tag{2.44}$$

where we have assumed that $\boldsymbol{u}^{(2)} = \boldsymbol{0}$ when $\boldsymbol{u}^{(1)} = \boldsymbol{0}$. The evolution equation (2.41) now becomes

$$\frac{\partial U}{\partial \tau} + \sigma \frac{\partial U}{\partial x} + \frac{l_i B_{1ijl} r_j r_l}{l_p r_p} U \frac{\partial U}{\partial x} - \left(\frac{2\alpha_\lambda + \gamma_\lambda}{2 l_p r_p} B_{\lambda jk} r_j r_k\right) U^2 \frac{\partial U}{\partial x} + \frac{l_i b_i}{l_p r_p} \frac{\mathrm{d}s_3}{\mathrm{d}x} = 0. \tag{2.45}$$

With the non-zero components of B_{ijl} given by (2.25), we construct from (2.40)

$$\boldsymbol{b} = \boldsymbol{c} = (l_1 r_1 + l_2 r_2,\, l_2 r_1,\, l_3 r_3 + l_4 r_4,\, l_4 r_3)^T, \tag{2.46}$$

$\boldsymbol{l}$ and $\boldsymbol{r}$ being given by (2.24). Then the weighting factors α_λ, γ_μ in (2.45) can be found by solving (2.42). The final form of the evolution equation is

$$\frac{\partial U}{\partial \tau} + \sigma \frac{\partial U}{\partial x} + \hat{\Gamma} U \frac{\partial U}{\partial x} - \Lambda U^2 \frac{\partial U}{\partial x} = -\beta \frac{\mathrm{d}s_3}{\mathrm{d}x}, \tag{2.47}$$

where $\hat{\Gamma} = \Gamma/\epsilon$, with Γ given by (2.26), and

$$\Lambda = \frac{3\alpha_\lambda B_{0\lambda jk} r_j r_k}{2 l_p r_p}, \tag{2.48}$$

$$\beta = \frac{v_{2c}}{2\left[v_{2c}\left(h_{1c} - v_{1c}^2\right) + v_{1c}\left(h_{2c} - v_{2c}^2\right)\right]}. \tag{2.49}$$

https://doi.org/10.1017/S0022112006004071 Published online by Cambridge University Press

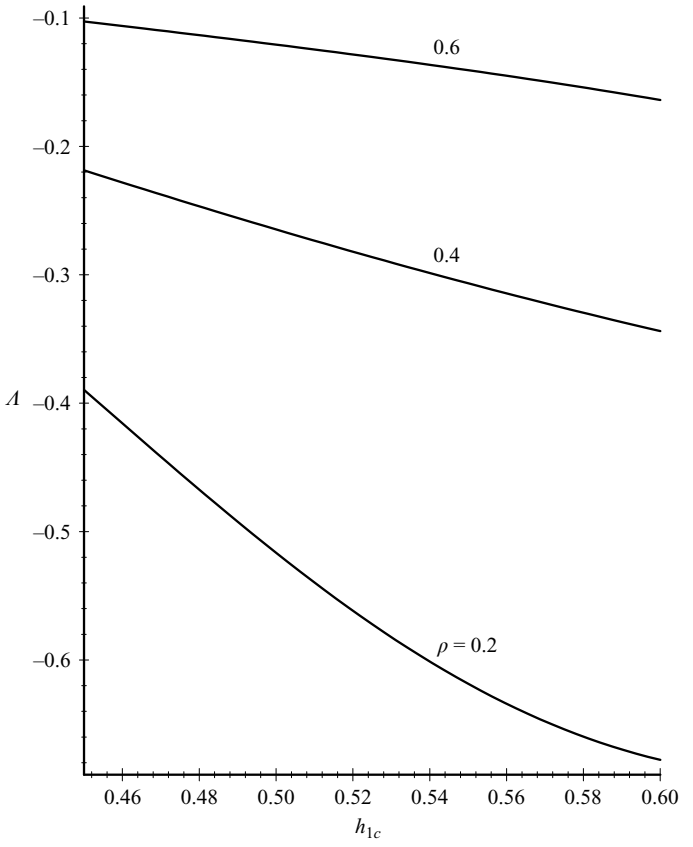


FIGURE 5. The coefficient Λ given by (2.48) for resonant internal-layer waves.

An explicit expression for Λ can be readily determined on first solving (2.42) for α_λ and substituting into (2.48). Specific details can be found in Cramer & Sen (1992) and Kluwick & Cox (1998). In figure 5 we plot $\Lambda(\rho, h_{1c})$ for critical flow conditions near the $\Gamma = 0$ transition curve, for the case where $v_{1c} = v_{2c} = v_c$ satisfies (2.18) and (2.20).

The evolution equation (2.47) for internal-layer waves clearly differs from (2.21) for surface-layer waves in the inclusion of a cubic nonlinear term involving the coefficient Λ. Waves can now steepen both backwards and forwards, allowing for the simultaneous occurrence of positive and negative hydraulic jumps in an evolving wave. As a result, evolution equations having a cubic as well as a quadratic nonlinearity are said to exhibit mixed nonlinearity and arise in a variety of applications describing for example acoustic waves in dense gases, elastic shear waves and density waves in fluidized beds (see Kluwick 1991*a*).

It is of interest to consider results for the limiting case where $1 - \rho \ll 1$. When the unperturbed flow velocities are the same in both fluid layers then the critical flow velocity is given from (2.18) by

$$v_c^2 = (1 - \rho) h_{1c} h_{2c} + O((1 - \rho)^2). \tag{2.50}$$

For this slow flow, the coefficients in (2.47) take the limiting values

$$\Gamma = \frac{3}{2h_{2c}} (h_{1c} - h_{2c}) v_c^2 + O\left(v_c^4\right), \tag{2.51}$$

https://doi.org/10.1017/S0022112006004071 Published online by Cambridge University Press

$$\Lambda = \frac{-3}{h_{2c}^2}\left(3h_{1c}^2 - 3h_{1c} + 1\right)v_c^3 + O\left(v_c^5\right), \tag{2.52}$$

$$\beta = \frac{1}{2} + O\left(v_c^2\right). \tag{2.53}$$

It is clear from (2.51) that the critical state $\Gamma = 0$ corresponds to equal depths in both fluid layers.

The evolution equation (2.47), with Γ, Λ and β given by (2.51)–(2.53), agrees with the results of Melville & Helfrich (1987) if dispersive effects included by them are neglected. While they consider the case where the upper fluid layer is assumed to have a rigid upper surface, this is a consistent approximation to a free surface when $1 - \rho \ll 1$.

3. Results

As mentioned in § 2, formal solution of the evolution equations (2.21) and (2.47) by means of the method of characteristics leads, in general, to the formation of regions of multivaluedness, which then have to be removed by the insertion of shock fronts representing hydraulic jumps.

The insertion of discontinuities into the solutions of scalar hyperbolic equations that are of the form (2.21) or (2.47) can be approached in a number of different but standard ways. For example, one can construct a travelling-wave solution based on a viscous regularization which gives the jump conditions in the limit of small viscosities. There is also the requirement of linearized stability where the shock is perturbed and where well-posedness of the perturbed problem leads to a jump condition. Alternatively, there is the evolutionary requirement that a smooth function asymptotic to the shock will evolve to the shock with increasing time. Whichever criterion is used, the jump conditions predicted are the same for a strictly convex (or concave) flux. So, for example, if (2.21) is interpreted as a conservation law for the density function U with flux function $j(U) = \sigma U + \Gamma U^2/2$, the above approaches are equivalent to the Lax shock condition

$$v_{wb} > v_s > v_{wa}, \quad v_w = j'(U), \quad v_s = \frac{[j]}{[U]}, \tag{3.1}$$

which is a geometric constraint on the characteristic slopes. Here $[A]$ denotes the jump of the quantity A, i.e. the difference between the values after and before the front; $[A] = A_a - A_b$. In the case of a non-convex flux such as in (2.47), where $j = \sigma U + \hat{\Gamma} U^2/2 - \Lambda U^3/3$, the Lax condition must be replaced by the Oleinik condition (Oleinik 1959)

$$\frac{j(U) - j(U_b)}{U - U_b} \geqslant v_s \quad \text{or} \quad v_s \geqslant \frac{j(U) - j(U_a)}{U - U_a}, \quad v_s = \frac{[j]}{[U]}, \tag{3.2}$$

which is required to hold for all U between U_a and U_b. This condition reduces to the Lax condition in the case of a convex flux. Shocks constructed in such a way that they satisfy the Oleinik condition are also admissible shocks by a mathematical entropy inequality, the viscosity criteria and the evolutionary criterion (see Hayes & LeFloch 1997).

The discussion of jump conditions presented so far has been based entirely on the evolution equations (2.21) and (2.47). From a physical point of view, however, a treatment on the basis of governing equations in integral form rather than in

https://doi.org/10.1017/S0022112006004071 Published online by Cambridge University Press

differential form appears to be more appropriate. As shown in Baines (1995) for the case of hydraulic jumps in a two-layer flow with a rigid upper lid, the three equations for conservation of mass in each layer and of momentum in both layers supplemented with a geometric constraint are not sufficient to solve for the downstream variables v_{1a}, h_{1a}, v_{2a}, h_{2a} if the upstream quantities and the speed of the jump are given. Obviously, this difficulty also arises in the case of the flow considered here, where the pressure at the (free) upper boundary is known but no geometric constraint is imposed. Various sets of assumptions have been proposed to close the set of equations. For example, in the work of Chu & Baddour (1977) and Wood & Simpson (1984) it was assumed that energy dissipation can occur only in an expanding layer. This allows the application of the Bernoulli equation to a contracting layer and, in turn, yields a fully conservative flow description. A different but again conservative closure has been considered more recently by Lowe, Rottman & Linden (2005). In an earlier work by Yih & Guha (1955) the interfacial pressure was assumed to vary linearily with the thickness of the upper layer and, thus, a separate equation for the conservation of momentum in the upper layer could be derived, which, however, was not in conservative form.

Assuming expansions of the fluid quantities as in § 2 and, in addition, of the bore speed W,

$$W = \epsilon W^{(1)} + \epsilon^2 W^{(2)} + O(\epsilon^3), \tag{3.3}$$

one then readily finds that the relationships (2.17) and (2.35) are consistent with all three closure assumptions mentioned earlier. Also,

$$W^{(1)} = \frac{[j]}{[U]} = v_s \tag{3.4}$$

in situations where $\Gamma = O(1)$, while

$$W^{(1)} = 0, \quad W^{(2)} = \frac{[j]}{[U]} = v_s \tag{3.5}$$

for internal-layer waves having $\Gamma = O(\epsilon)$. As a result, we conclude that the jump relationships (3.1) and (3.2), which are consistent with the evolution equations (2.21) and (2.47), are consistent also with formulations of the governing equations in integral form proposed in the literature. In view of the fact that the bores considered in the present context are weak bores, this may not be too surprising and it is also for this reason that details of the derivation have been suppressed.

Compared with the case of a convex flux, the case of a non-convex flux provides new physical phenomena (see the review paper by Kluwick 2001). In particular, in the context of gas-dynamics there is the formation of compound shock-fan structures, where the fan is attached to the shock. We adopt, from gas-dynamics, the terminology 'sonic shock' used to denote a shock travelling at a characteristic sound speed (given by the signal at the attached edge of the fan).

The consequence of the above discussion is that a hydraulic discontinuity (either jump or fall) propagating in (2.21) must satisfy the Lax criterion. Solutions of this transport equation for weakly nonlinear shallow-water waves with $\Gamma = O(1)$ were obtained by Grimshaw & Smyth (1986) and in the different context of unsteady transonic nozzle flows by Kluwick (1972), Adamson & Richey (1973) and Kluwick & Scheichl (1996). In the following, therefore, we shall concentrate on the non-convex case (2.47), i.e. hydraulic internal-layer waves having $\Gamma = O(\varepsilon)$. For the time being, we will also assume that jumps satisfy the Oleinik condition (3.2), enabling the formation

https://doi.org/10.1017/S0022112006004071 Published online by Cambridge University Press

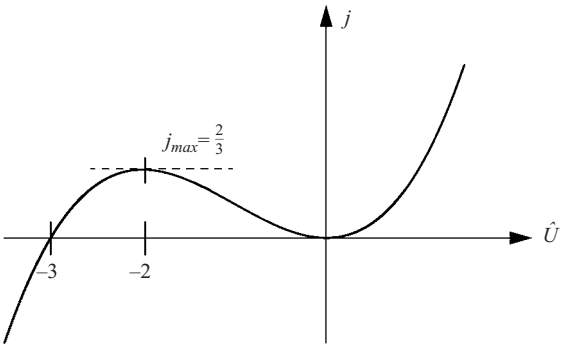


FIGURE 6. Flux function $j(\hat{U})$.

of so-called sonic jumps, which influence the flow field by the generation of waves initially travelling with the same speed as the jump itself. A more detailed discussion concerning the applicability of condition (3.2) if the internal jump structure is assumed to be affected not only by viscosity but, equally, also by dispersion is presented in § 4. There it will be shown that if the ratio of dissipation and dispersion falls below a certain value, then even non-sonic jumps may form which emanate rather than absorb waves (non-classical discontinuities).

The transport equation (2.47) has to be solved numerically in general. Before doing so it is, however, convenient to eliminate the parameters $\hat{\Gamma}$, Λ and β by introducing suitably scaled quantities $\hat{U}$, $\hat{X}$ and S in place of U, x and s_3:

$$\hat{U} = -\frac{2\Lambda}{\hat{\Gamma}}U\,, \quad \hat{X} = -\frac{2\Lambda}{\hat{\Gamma}^2}x\,, \quad S = \frac{4\beta\Lambda^2}{\hat{\Gamma}^3}s_3. \tag{3.6}$$

In order to simplify the calculations, the detuning parameter σ is set to 0. One then obtains the normalized transport equation

$$\frac{\partial\hat{U}}{\partial\tau} + \hat{U}\frac{\partial\hat{U}}{\partial\hat{X}} + \frac{1}{2}\hat{U}^2\frac{\partial\hat{U}}{\partial\hat{X}} = -\frac{\mathrm{d}S}{\mathrm{d}\hat{X}}. \tag{3.7}$$

It should be noted that the definition of $\hat{X}$ leaves the propagation direction unchanged as Λ is a strictly negative quantity (see figure 5) and $\hat{\Gamma}$ enters in quadratic form only. In contrast, the shape function $\hat{U}$ and the forcing function S change sign if $\hat{\Gamma}$ changes sign. By introducing the flux

$$j = \frac{\hat{U}^2}{2} + \frac{\hat{U}^3}{6}, \tag{3.8}$$

(3.7) assumes the conservative form

$$\frac{\partial\hat{U}}{\partial\tau} + \frac{\partial j}{\partial\hat{X}} = -\frac{\mathrm{d}S}{\mathrm{d}\hat{X}}. \tag{3.9}$$

For the cubic flux function from (3.8), the Oleinik criterion (3.2) can be written as

$$v_{wb} > v_s \geqslant v_{wa} \tag{3.10}$$

and thus turns out to be equivalent to the Lax wave-speed-ordering principle (3.1) in the generalized sense that for the downstream state the equality sign has to be included (sonic jumps).

The graph $j(\hat{U})$ depicted in figure 6 exhibits a minimum, $j_{min} = 0$, as well as a maximum, $j_{max} = 2/3$. This is in sharp contrast with the classical cases of free-surface-layer

https://doi.org/10.1017/S0022112006004071 Published online by Cambridge University Press

waves or internal-layer waves having strictly positive or negative nonlinearity, where the flux function exhibits a single minimum or maximum.

In the case of steady flow, which will be investigated first, (3.9) can immediately be integrated to yield

$$j(\hat{U}(\hat{X})) + S(\hat{X}) = Q, \tag{3.11}$$

where the integration constant Q characterizes the deviation of the flux from the value associated with unperturbed critical flow conditions.

Equation (3.11) can be used to design a surface topography which produces a prescribed distribution $\hat{U}(\hat{X})$ or to calculate $\hat{U}(\hat{X})$ for a given shape $S(\hat{X})$ of a surface-mounted obstacle. In this connection it is useful to recognize a simple geometrical interpretation of (3.11): the surface elevation $S(\hat{X})$ corresponding to a specific value $\hat{U}$ is given by the distance between the line $j = Q$ and the $j(\hat{U})$ plot.

As a first example, let us construct the bottom topography that yields linear distributions of the perturbation quantities

$$\hat{U} = C\hat{X} \quad \text{for} \quad \hat{X} < 3 \tag{3.12}$$

and

$$\hat{U} = 3C \quad \text{for} \quad \hat{X} \geqslant 3. \tag{3.13}$$

Combining (3.8) and (3.11) then gives the required surface elevation

$$S = \begin{cases} Q - \dfrac{C^2\hat{X}^2}{2} - \dfrac{C^3\hat{X}^3}{6}, & \hat{X} < 3, \\ Q - \dfrac{9C^2}{2} - \dfrac{9C^3}{2}, & \hat{X} \geqslant 3. \end{cases} \tag{3.14}$$

In agreement with our earlier geometrical considerations, the shape of the bottom surface is obtained by inverting the $j(\hat{U})$ graph and applying a shift Q in the normal direction. As a result, the bottom topography exhibits a local maximum as well as a local minimum, as shown in figure 7(*a*) for $Q = 0$, $C = -1$. The results are displayed in figure 7(*b*). The notation 'subcritical' and 'supercritical' used in figure 7(*b*) is meant to indicate that small perturbations of the steady flow field at the point under consideration will be convected upstream and downstream, i.e. $v_w < 0$ and $v_w > 0$. Also included in figure 7(*b*) are solutions for the same topography but values of Q different from zero, for which it generates the imposed linear distributions (3.12) and (3.13). The general form of the solutions is understood most easily by recognizing that each maximum or minimum of the j versus $\hat{U}$ relationship leads to the formation of critical points (nodes and saddle points) at $\hat{X}$ locations having $S'(\hat{X}) = 0$. As an immediate consequence of this result, and following from the geometrical interpretation of (3.11), one reaches the interesting conclusion that the solution of the steady flow problem for $Q = 0$ is not unique. In addition to the imposed continuous distribution of $\hat{U}$, there exists a second solution with identical behaviour upstream and downstream. This second solution contains a jump discontinuity, which, according to the Oleinik criterion, occurs in the form of a sonic negative hydraulic jump as shown in figure 7(*b*).

Next let us investigate steady flows associated with a single isolated hump or indentation. Specifically, we consider surface-mounted obstacles of the form

$$S(\hat{X}) = \frac{\sigma}{\cosh^2 \hat{X}}, \tag{3.15}$$

where σ characterizes the maximum height or depth. Representative results for $\sigma > 0$ are plotted in figures 8–10.

https://doi.org/10.1017/S0022112006004071 Published online by Cambridge University Press

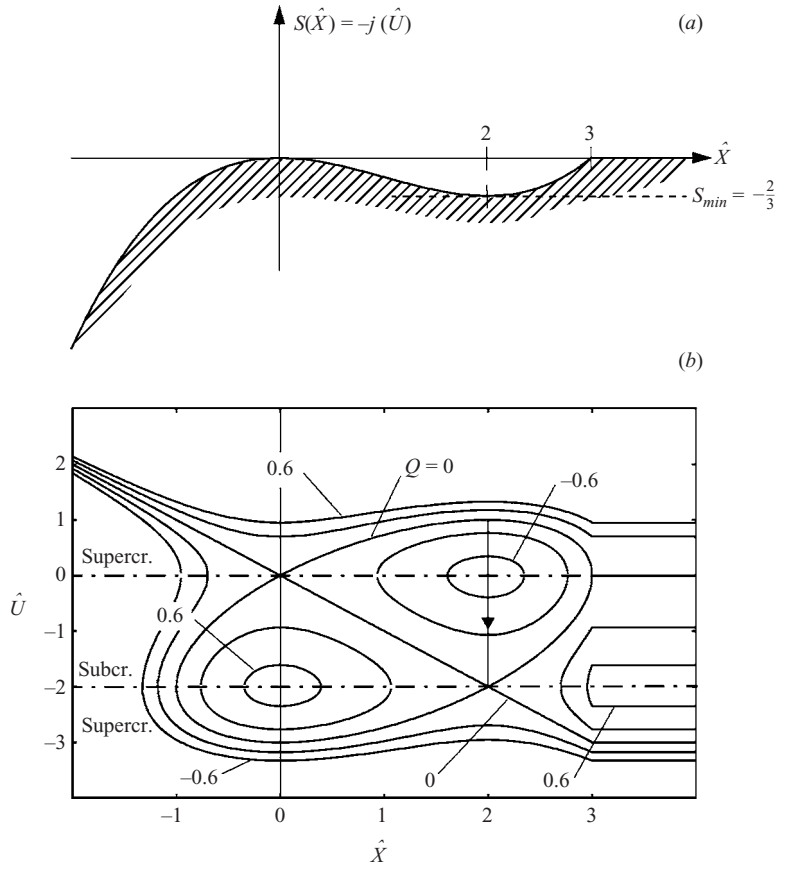


FIGURE 7. (*a*) Bottom topography S yielding a linear distribution of $\hat{U}$ for $Q = 0$. (*b*) Distributions of $\hat{U}$ for various values of Q.

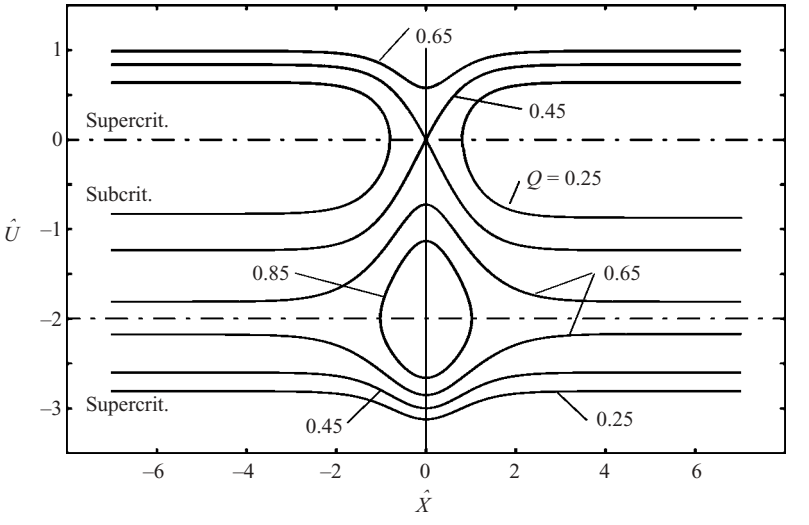


FIGURE 8. Flow past a single hump: distributions of $\hat{U}$ for various values of Q and $\sigma = 0.45$.

https://doi.org/10.1017/S0022112006004071 Published online by Cambridge University Press

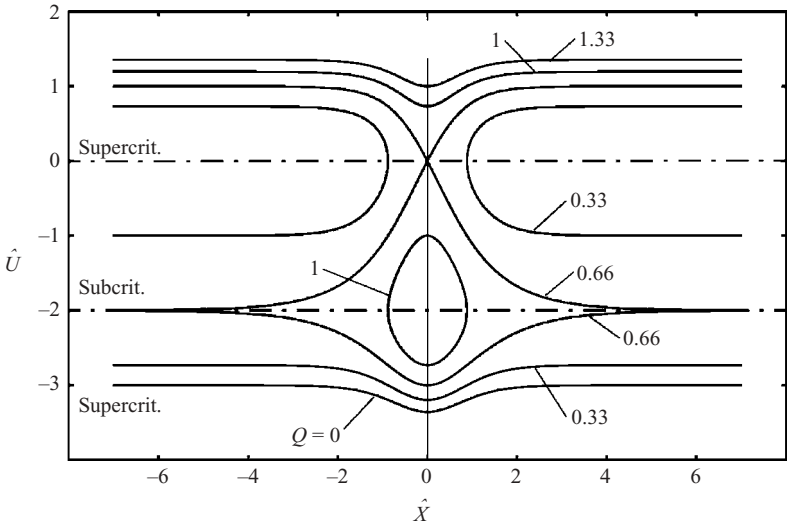


FIGURE 9. Flow past a single hump: distributions of $\hat{U}$ for various values of Q and $\sigma = 0.66$.

If $\sigma < j_{max} = 2/3$, as in figure 8, there exist two ranges of the perturbation flux, $Q > \sigma$ and $Q < j_{max}$, of purely supercritical flow and a range $j_{max} > Q > \sigma$ of purely subcritical flow. Furthermore, as in the classical case of strictly positive nonlinearity, a transition from subcritical to supercritical and supercritical to subcritical flow is possible for a specific value, $Q = \sigma$. In addition, there exist solutions having $Q < \sigma$ which cannot be continued up to and beyond the crest of the hump and, therefore, are of no physical relevance. Finally, note that the second supercritical flow regime, with $Q < j_{max}$, generates disturbances $U > \hat{\Gamma}/\Lambda$ and, consequently, loses its significance in the limit $\hat{\Gamma} \to \infty$ of strictly positive nonlinearity.

As the height of the hump σ increases, the range of the perturbation flux allowing purely subcritical flow narrows, and vanishes if σ assumes the value j_{max}. As shown in figure 9, possible solutions then include purely supercritical flows with $Q > j_{max}$ and $Q < j_{max}$ and flows having $Q = j_{max}$ and leading from subcritical to supercritical conditions or vice versa.

If the height σ of the obstacle increases further, i.e. exceeds the value j_{max}, the qualitative properties of steady flow change again as indicated in figure 10, where we consider the case $\sigma = 1$. As before, there exist two ranges of the perturbation flux Q for which purely supercritical flows are possible ($Q > \sigma$ and $Q < j_{max}$), while purely subcritical flows do not exist. In contrast with the results depicted in figure 7, however, solutions which describe the transition from a subcritical to a supercritical state or a supercritical to a subcritical state can no longer be constructed. This is due to the fact that two of the branches leaving the saddle point form a closed loop which encloses the node. Owing to the existence of this loop, the flow with $Q = \sigma$, which has both a supercritical upstream and supercritical downstream state, is no longer unique. In addition to the continuous solution, which assumes critical flow conditions at $\hat{X} = 0$, there exists a second solution, which exhibits two jump discontinuities. First, there is a negative hydraulic jump located upstream of $\hat{X} = 0$, which leads from supercritical to critical flow conditions if the Oleinik criterion holds as assumed earlier. Further downstream, the two-layer fluid returns to supercritical conditions before it jumps

https://doi.org/10.1017/S0022112006004071 Published online by Cambridge University Press

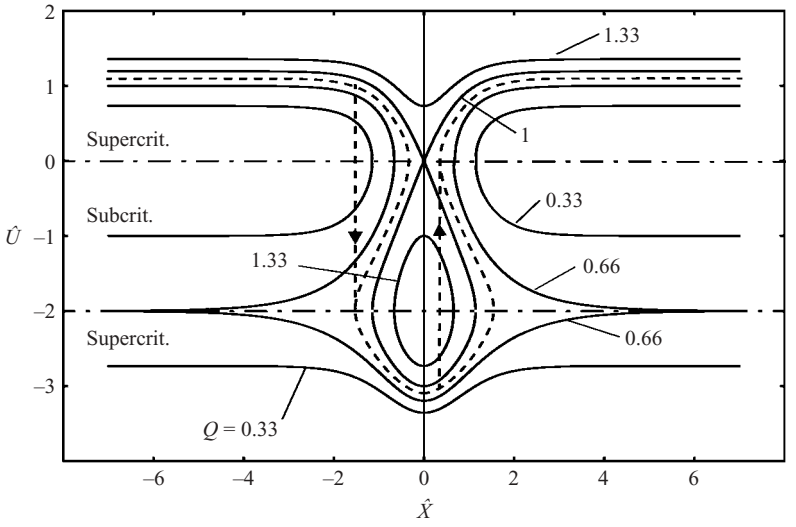


FIGURE 10. Flow past a single hump. Distributions of $\hat{U}$ for various values of Q and $\sigma = 1$.

back to a critical state by means of a second positive hydraulic jump at $\hat{X} = 0$. For $\hat{X} > 0$, the continuous and discontinuous solutions coincide.

The non-uniqueness of the flow with $Q = 1$ raises the question which of the two possible solutions will occur in reality. Inspection of neighbouring solutions, as for example the one given by the dashed line in figure 10, reveals that flows with a slightly smaller value of Q will always contain two hydraulic jumps, a sonic negative jump upstream of $\hat{X} = 0$ and a sonic positive jump downstream of $\hat{X} = 0$. This suggests that the solution with two hydraulic jumps can be realized physically by slowly increasing the perturbation flux from $Q < 1$ to $Q = 1$. In contrast, the continuous solution will be of relevance if the perturbation flux is slowly reduced from a value $Q > 1$ to $Q = 1$.

A different way to reach this conclusion is to investigate directly the stability of the continuous steady-state solution with respect to changes in Q, which is of interest also in its own right. Specifically, we assume that the flow field at time $\tau = 0$ is given by the continuous solution with $Q = 1$ and investigate the changes which arise if $\hat{U}$ far upstream of the hump is slightly reduced to about the value associated with the dotted curve in figure 10 for all times $\tau > 0$. The evolution of the resulting disturbances was calculated numerically using a Godunov scheme suitably designed for conservation laws with non-convex flux functions (see LeVeque 1992). The results are depicted in figure 11.

Since the flow upstream of the hump is supercritical, the disturbances are convected downstream initially. Owing to the fact, however, that the unperturbed continuous steady solution has a critical state at $\hat{X} = 0$, they cannot reach the crest of the hump in finite time. Furthermore, as the amplitude of the disturbances increases, thereby generating subcritical flow conditions eventually, they start to propagate upstream. This in turn causes the formation of a negative hydraulic jump moving upstream also, as long as the corresponding downstream state is subcritical. Finally, however, the disturbances immediately downstream of this hydraulic jump are large enough to reach a critical state and, as a result, it ceases to move upstream and assumes a steady-state position in finite time. The disturbances downstream of the sonic hydraulic jump

https://doi.org/10.1017/S0022112006004071 Published online by Cambridge University Press

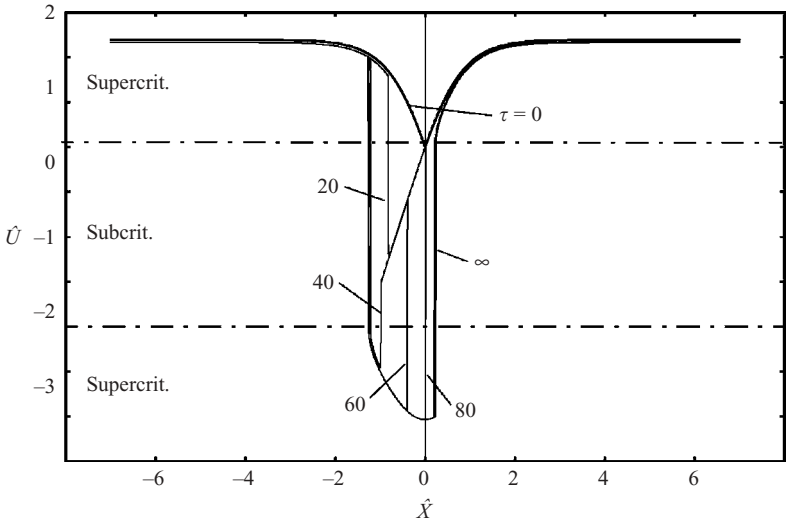


FIGURE 11. Flow past a single hump. Stability of the steady solution $\hat{U}$ for $Q = 1$ and $\sigma = 1$. Distributions are shown for various values of τ.

still grow. They enter the supercritical regime, therefore, and propagate downstream, which leads to the formation of a positive hydraulic jump. This discontinuity moves downstream initially but also approaches a steady-state position as critical flow conditions immediately downstream of the front are reached asymptotically in the limit $\tau \to \infty$. We thus again conclude that the continuous steady solution with $Q = 1$ is unstable with respect to small decreases in the perturbation flux.

As a second example involving unsteady effects, we investigate how a steady two-layer flow past a single hump of the form (3.15) which is subcritical far upstream and downstream but reaches a critical state at $\hat{X} = 0$ is transformed into a flow leading from subcritical to supercritical conditions by the imposition of appropriate boundary conditions at some location $\hat{X} = \hat{X}_0 > 0$. Specifically, we assume that $\sigma = j_{max} = 2/3$ and that $\hat{U}$ is rapidly increased at $\hat{X} = 7$ from -2 at $\tau = 0$ to 0 at $\tau = 1$, i.e. over a time interval $\Delta\tau = 1$. Results obtained by numerical integration of the evolution equation (3.7) are plotted in figure 12.

The rapid increase in $\hat{U}$ imposed at $\hat{X}_0 = 7$ causes the formation of a positive hydraulic jump, which propagates upstream. It weakens with increasing time and vanishes before it reaches the crest of the hump located at $\hat{X} = 0$. The possibility that a jump discontinuity may terminate at finite time was predicted first by Kluwick & Czemetschka (1990) (see also Kluwick 1991*a*) in the context of weakly nonlinear spherical and cylindrical acoustic waves in dense gases. This sudden 'death' of a hydraulic jump represents another non-classical feature of the type of flow considered here. In the case of free-surface-layer waves and internal-layer waves with strictly positive or negative nonlinearity, hydraulic jumps, once generated, live forever; they weaken as time progresses, but they never 'die'.

The 'death' of the upstream-moving hydraulic jump results in a continuous distribution of $\hat{U}$. The disturbances propagate with the local wave speed and thus cannot pass beyond the crest of the hump, where the unperturbed flow has a critical state $\hat{U} = 0$. Consequently, the wave is reflected, leading in turn to the occurrence of a negative hydraulic jump with supercritical flow conditions upstream of the front. It

https://doi.org/10.1017/S0022112006004071 Published online by Cambridge University Press

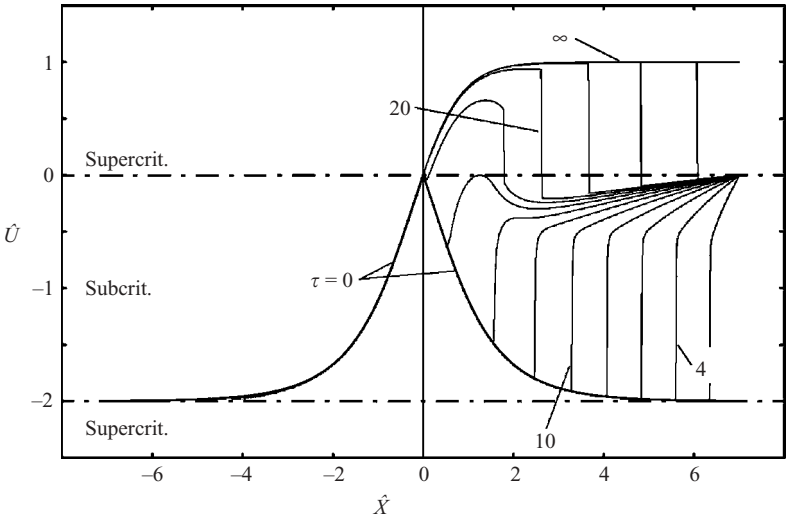


FIGURE 12. Flow past a single hump. Transition from a purely subcritical to a subcritical–supercritical flow for $\sigma = 0.66$. Distributions are shown for various values of τ; $\Delta\tau = 1$.

is swept downstream, thus generating the desired steady transition from a subcritical to a supercritical state asymptotically in the limit $\tau \to \infty$.

As pointed out before, the surface topography (3.14) admits two different solutions for a given value of Q (figure 7*b*). In addition to the desired piecewise-linear distribution (3.12), (3.13) of $\hat{U}$, there exists a second solution, which contains a negative hydraulic jump located at the local minimum of $S(\hat{X})$. This raises the question which of these solutions will be realized in a start problem similar to the investigation for a hump of the form (3.15) and $\sigma = j_{max}$. Integration of the evolution equation (3.7) with respect to $\hat{X}$ along the characteristics $\xi = \text{constant}$ with $\mathrm{d}\hat{X}/\mathrm{d}\tau = v_w$ yields the compatibility condition

$$j(\hat{U}(\hat{X}, \xi)) + S(\hat{X}) = f(\xi), \tag{3.16}$$

which differs from its steady counterpart (3.11) only insofar as the integration constant Q is replaced by a function of ξ. This implies that, on each characteristic $\xi = \text{constant}$, j and S are related in exactly the same way as in the case of steady flow. Consequently, we conclude that the portion of the linear distribution (3.12) that is located inside the loop branching off the saddle points situated at the local maximum $\hat{X}_{max}$ and the local minimum $\hat{X}_{min}$ of the topography (3.14), respectively, cannot be generated by characteristics emanating from the downstream boundary $\hat{X} = \hat{X}_0$. Therefore, we expect that the steady solution with a hydraulic jump rather than the continuous solution will be realized by the type of transition process considered here.

As shown in figure 13, this conclusion is in agreement with the numerical computations. Starting with the solution for $Q = 0$ having a supercritical state at $\hat{X}_{min}$ and a critical state at $\hat{X}_0$, the quantity $\hat{U}$ at the downstream boundary $\hat{X} = \hat{X}_0$ was lowered continuously (within the time interval $\Delta\tau = 1$) starting from 0 until it assumed the value -2. Since the flow properties upstream of $\hat{X}_{min}$ remain unaffected by the boundary conditions imposed at $\hat{X} = \hat{X}_0 = 4$ for all times, the flow regime displayed in figure 13 is limited to $\hat{X} \geqslant 2$.

The reduction of $\hat{U}$ below 0 leads to subcritical flow conditions at $\hat{X} = \hat{X}_0$. The disturbances generated at the downstream boundary propagate upstream, therefore,

https://doi.org/10.1017/S0022112006004071 Published online by Cambridge University Press

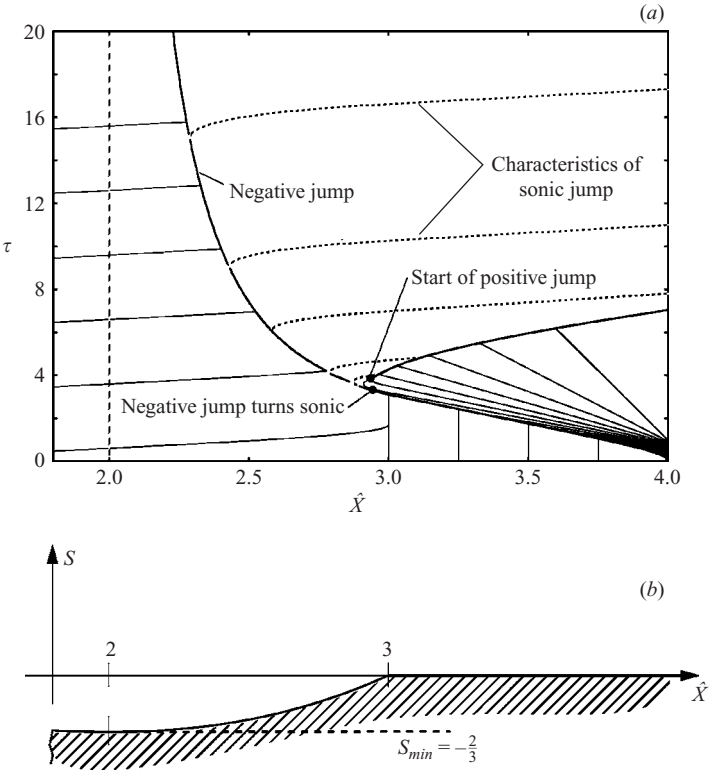


FIGURE 13. (*a*) Characteristic curves (thin and dotted lines) and jump discontinuities associated with the transition process leading from supercritical flow conditions to a steady solution with a negative hydraulic jump; $\hat{X}_0 = 4$, $\Delta\tau = 1$. For the meaning of the dashed line see the main text. (*b*) Bottom topography S as in figure 7(*a*).

thereby generating a negative hydraulic jump. Its strength increases with increasing time and it assumes a sonic (critical) downstream state at $\tau_{son} \approx 3$. For $\tau \geqslant \tau_{son}$ the discontinuity emanates characteristics in the tangential direction and slowly approaches its steady-state position in the limit $\tau \to \infty$. Since the flow immediately after the hydraulic jump is subcritical, the emanating characteristics move upstream initially. With increasing time, therefore, $S(\hat{X})$ decreases, which in turn forces the flux j to increase according to the compatibility relationship (3.16). As a consequence, critical flow conditions $j = 2/3$ with $v_w = 0$ are reached on each of these characteristics for the specific values $\hat{X} = \hat{X}_*(\xi)$, $\tau = \tau_*(\xi)$. As τ increases beyond τ_*, the flow quantities on the characteristic $\xi = \text{constant}$ under consideration then enter the supercritical flow regime $\hat{U} < -2$ and the wavefront is swept downstream. This causes the formation of a positive hydraulic jump, which eventually leaves the flow domain and, more importantly, generates the supercritical portion of the linear steady-state distribution (3.12), (3.13) of $\hat{U}$ downstream of the sonic negative hydraulic jump located at $\hat{X} = 2$.

What is clear from these solutions is the new phenomena that arise owing to the non-convex flux (or mixed nonlinearity). We have the coexistence of positive and negative hydraulic jumps and propagating sonic jumps. In a novel evolution problem we have shown how the transition from one steady state to another can be achieved by upstream-propagating waves. The mechanism for transition from a subcritical to

https://doi.org/10.1017/S0022112006004071 Published online by Cambridge University Press

a supercritical state is accomplished only through an upstream-propagating hydraulic jump terminating in finite time with the formation of a stable negative hydraulic jump moving downstream. This scenario has no counterpart in theories based on convex flux functions.

4. Further comments on shock admissibility

Following the discussion of some specific flow problems let us return to the more fundamental question of shock admissibility. As shown more recently for non-convex flux functions, some weak solutions satisfying an admissible mathematical-entropy inequality may violate the Oleinik geometric conditions (see Hayes & LeFloch 1997). These solutions have furthermore been shown to be stable. The key idea to their construction is that they arise when the hyperbolic equation is embedded in a structure involving not just viscosity but also dispersion. These shocks then are generated as limits of diffusive–dispersive travelling waves and are termed non-classical shocks. Each jump can thus be regarded as representing a dissipative–dispersive profile whose streamwise extent is so small compared with the characteristic wavelength that it collapses into a single point. Such shocks have a greater strength than that allowed for classical shocks satisfying condition (3.10), as they involve characteristics emanating from one side of the shock rather than intersecting the shock path. The non-classical feature of these shocks is also related to their structural sensitivity – the shock strength itself depends on the precise ratio of dispersion and dissipation in the system.

Figure 14(*a*) displays the $\hat{U}$ versus j diagram. It then follows immediately from the relationships (3.1) for the wave speed v_w and the shock speed v_s that the slopes of a wavefront or a shock front in the $(\hat{X}, \tau)$-plane are given by the slope of the tangent to this graph at the point under consideration or by the slope of the so-called Rayleigh line, i.e. the chord which connects the upstream and downstream states.

For example, if we consider a hydraulic jump leading from state 1 to state 2, we obtain a Lax-shock scenario, depicted in figure 14(*b*), i.e. a jump discontinuity and merging wavefronts. If the value of $\hat{U}$ downstream of the discontinuity is reduced, we eventually reach the limiting case of a sonic hydraulic jump characterized by the property that the shock front is parallel to the wavefront immediately downstream of the discontinuity. According to the Oleinik criterion (3.10), this sonic discontinuity represents the hydraulic jump of maximum possible strength if the upstream state 1 is fixed (figure 14*c*). If we consider stronger hydraulic jumps, for example the jump connecting states 1 and 4, we obtain the configuration of a so-called undercompressive shock shown in figure 14(*d*). The downstream wavefront now leaves the discontinuity rather than merging with it, which, in general, is considered as inadmissible. However, this may not be so if dispersive effects, which have been neglected so far, are taken into account. This is seen most easily by investigating the model equation

$$\frac{\partial \hat{U}}{\partial \tau} + \left(1 + \frac{\hat{U}}{2}\right)\hat{U}\frac{\partial \hat{U}}{\partial \hat{X}} = \alpha \frac{\partial^2 \hat{U}}{\partial \hat{X}^2} + \gamma \frac{\partial^3 \hat{U}}{\partial \hat{X}^3}, \quad \alpha > 0, \tag{4.1}$$

i.e. the transport equation (3.7) derived earlier for a locally flat bottom, $S \equiv 0$, augmented with standard dissipative and dispersive terms. This equation is similar to the dispersive equations for two-layer flows considered by for example Kakutani & Yamasaki (1978), Melville & Helfrich (1987) and Grimshaw, Pelinovsky & Talipova (1997) but now we will consider a specific viscous dissipation of the form used in the

https://doi.org/10.1017/S0022112006004071 Published online by Cambridge University Press

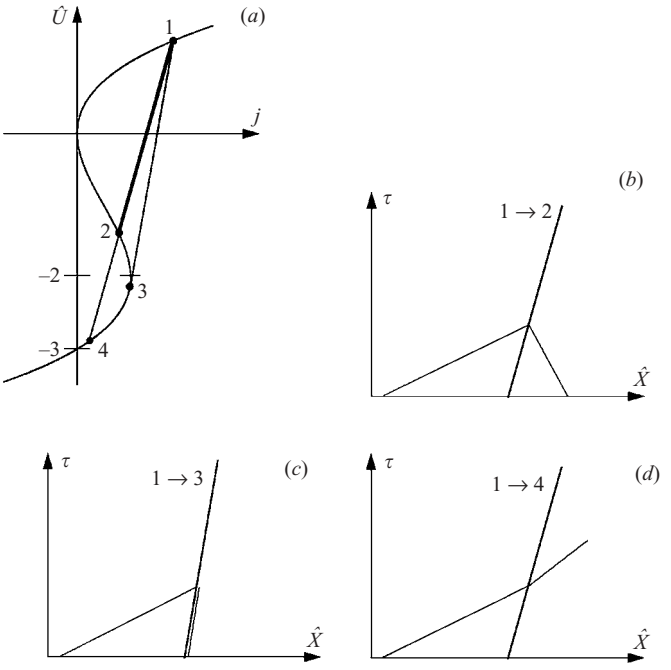


FIGURE 14. Oleinik criterion: (*a*) Graph of the flux function $j(\hat{U})$ given by (3.8) including straight lines (Rayleigh lines) connecting upstream and downstream states of jumps. (*b*) Admissible jump, $1 \to 2$. (*c*) Jump of maximum possible strength (sonic shock), $1 \to 3$. (*d*) Inadmissible jump (undercompressive shock), $1 \to 4$.

papers by Schär & Smith (1993) and Smith & Smith (1995) (see also Jiang & Smith 2001*a*, *b*; Gustafsson & Sundstrom 1978). In this connection, it should be added that purely dispersive limits of continuously stratified flows were investigated by Clarke & Grimshaw (1994); Clarke & Grimshaw (1999, 2000). We also note that (4.1) without a cubic nonlinear term was proposed by Whitham (1974, p. 482) as a model for the internal structure of hydraulic jumps in single-layer fluids. Furthermore, it should be mentioned that if the effects of surface tension are assumed to be negligible small, the parameter γ is a strictly positive quantity (e.g. Melville & Helfrich 1987). However, as shown by Lighthill (1978) in the context of ripple propagation, the influence of the surface tension $\tilde{\sigma}$ has to be taken into account if the ratio $\tilde{\sigma}/[\tilde{\rho}_2\tilde{g}(\tilde{h}_{10}+\tilde{h}_{20})^2]$ becomes an $O(1)$ quantity. Then the dispersion relationship might be altered significantly in such a way that γ becomes negative. Therefore, this case will also be discussed in the following.

Finally, we draw attention to the recent paper by Stastna & Peltier (2005) on the generation of large-amplitude internal solitary and solitary-like waves. In contrast with the present study, where no restrictions on the density ratio are imposed, the calculations were based on the Boussinesq approximation but allowed for an arbitrary wave amplitude. The results clearly show that even waves of maximum amplitude cause only small displacements of the interface if the interface thickness is close to one-half the total fluid-layer thickness, i.e. if the nonlinear parameter Γ plotted in figure 3 is small, indicating in turn that a weakly nonlinear analysis is fully self-consistent.

As pointed out recently by Kluwick (1991*b*), (4.1) also arises in studies dealing with the evolution of weakly nonlinear, weakly dissipative and weakly dispersive

https://doi.org/10.1017/S0022112006004071 Published online by Cambridge University Press

kinematic waves in suspensions of particles in liquids, if the unperturbed state differs only slightly from the state associated with the inflexion point of the drift–flux relationship. The original equation (3.7) then is recovered in the limit of vanishing dissipation and dispersion, $\alpha \to 0$, $\gamma \to 0$.

In order to decide which shock discontinuities are admissible in this limit, Kluwick *et al.* (2000) studied travelling-wave solutions of (4.1):

$$\left.\begin{aligned} \hat{U} = \hat{U}(\xi), \quad \xi = \hat{X} - v_s\tau, \\ \hat{U} \to \hat{U}_b \quad \text{for} \quad \xi \to -\infty, \\ \hat{U} \to \hat{U}_a \quad \text{for} \quad \xi \to \infty, \end{aligned}\right\} \tag{4.2}$$

where $\hat{U}_b$ and $\hat{U}_a$ denote, respectively, the values of $\hat{U}$ before and after the shock. Introducing suitably scaled quantities G and η in place of U and ξ,

$$G = \frac{2}{[\hat{U}]}\left(\frac{\hat{U}_b + \hat{U}_a}{2} - \hat{U}\right), \quad \eta = \frac{[\hat{U}]^2}{24\alpha}\xi, \tag{4.3}$$

the shock-structure problem assumes the form

$$\left.\begin{aligned} (G^2 - 1)(B + G) = G' + DG'', \\ G \to \pm 1 \quad \text{for} \quad \eta \to \mp\infty, \end{aligned}\right\} \tag{4.4}$$

where a prime denotes differentiation with respect to η and

$$B = -\frac{6}{[\hat{U}]}\left(1 + \frac{\hat{U}_b + \hat{U}_a}{2}\right), \quad D = \frac{\gamma[\hat{U}]^2}{24\alpha^2}. \tag{4.5}$$

The definition of D indicates immediately how the limit to the non-dissipative non-dispersive case has to be carried out: by letting α and γ approach zero with γ/α^2 kept fixed. In this limit, ξ tends to zero almost everywhere, i.e. in the original variables the shock layer collapses into a jump discontinuity. Investigation of the shock-layer problem (4.4) shows that solutions do not exist for arbitrary values of the parameters B and D but only in a certain domain of the (B, D)-plane, as indicated in figure 15.

If $|D|$ is sufficiently large and D is negative, i.e. if $\gamma < 0$, the downstream state is approached monotonically while the upstream state is approached in an oscillatory manner. On increasing D, solutions are located in region II, for which both the downstream and upstream states are approached monotonically. A further increase in D leads into a third flow regime, III, where the departure from the upstream state is monotonic while the approach to the downstream state is oscillatory. In region I, shock-layer solutions exist for $B \geqslant 1$ only and shocks with $B = 1$ can be shown to have sonic downstream states. As a consequence, the Oleinik admissibility criterion is found to be satisfied. As shown by Kluwick *et al.* (2000), however, in regions II and III shock-layer solutions can be obtained for $B \geqslant B_{cr}(D)$ only where $B_{cr} > 1$ for $D > 0.5$. Moreover, shocks of limiting strength $B = B_{cr}(D) > 1$ are stronger than sonic shocks. Therefore they violate the Oleinik criterion, although they are clearly admissible owing to the existence of a shock-layer solution.

Figure 16 displays the behaviour of the solutions to the shock-layer problem (4.4) as B tends to B_{cr} with D fixed. In this limit, the shock layer is seen to split effectively into two sublayers. Inside the first sublayer G decreases from 1 to a value $-B_{cr}$ which is smaller than its value far downstream and inside the second sublayer increases to -1 to satisfy the downstream boundary condition. The sublayers are separated by a pronounced plateau region where $G \sim -B_{cr}$, whose length tends to infinity as B

https://doi.org/10.1017/S0022112006004071 Published online by Cambridge University Press

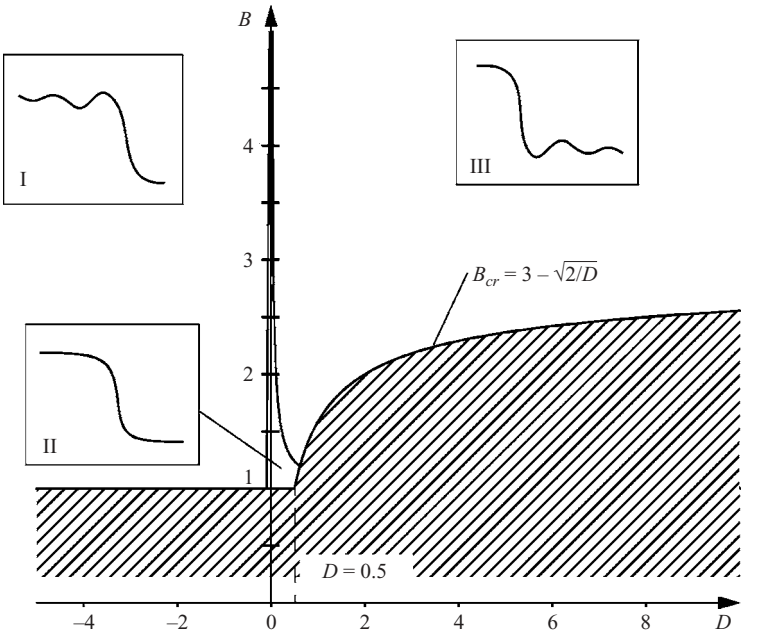


FIGURE 15. Combinations of B and D leading to different flow regimes. For (B, D)-pairs inside the shaded region, shock-layer solutions do not exist.

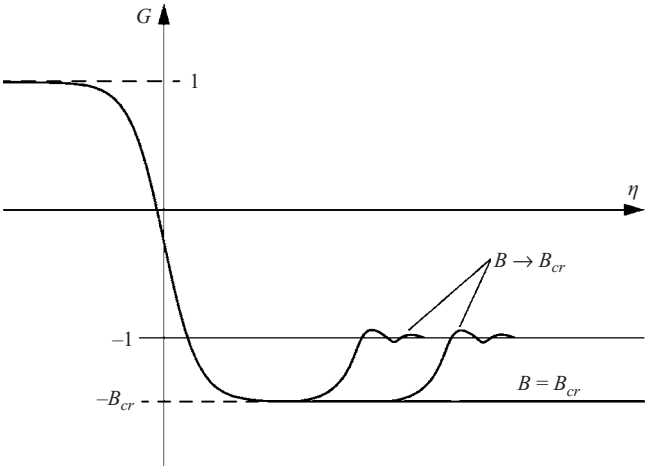


FIGURE 16. Solution to the shock-layer problem in the limit $B \to B_{cr}$.

approaches B_{cr}. In this limit we are left, therefore, with the profile inside the first sublayer. It can be calculated analytically,

$$\left.\begin{gathered} D > \frac{1}{2}, \\ G \sim \frac{1}{2}\left[1 - B_{cr} - (1 + B_{cr}) \tanh\left(\frac{(3 - B_{cr})(1 + B_{cr})}{4}(\eta + \text{const.})\right)\right], \\ B_{cr}(D) = 3 - \sqrt{\frac{2}{D}}, \end{gathered}\right\} \tag{4.6}$$

https://doi.org/10.1017/S0022112006004071 Published online by Cambridge University Press

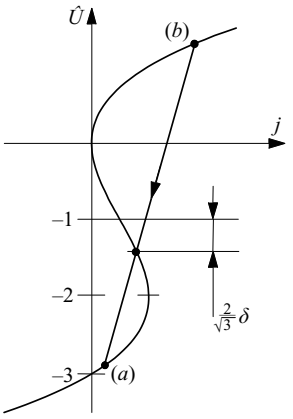


FIGURE 17. Non-classical shock $\hat{U}_b \to \hat{U}_a$ in the $(j, \hat{U})$-diagram.

and has a larger amplitude than a sonic shock with $B_{cr} = 1$. As a consequence, the wave and shock speeds will satisfy the ordering relationship

$$v_{wb} > v_s \leqslant v_{wa} \tag{4.7}$$

as in figure 14(d), rather than the Oleinik admissibility criterion. The subscript a now denotes the value after the non-classical shock, i.e. the value corresponding to $G = -B_{cr}$.

We note that the Rayleigh lines of such non-classical shocks, which emanate rather than absorb wavefronts, can easily be constructed in the $(j, \hat{U})$-diagram. As shown in Kluwick *et al.* (2000), all Rayleigh lines which characterize admissible non-classical shocks pass through fixed points that are a distance $2\delta/\sqrt{3}$, $\delta = \alpha/\sqrt{\gamma}$, from the inflexion point at $\hat{U} = -1$ in the $\hat{U}$ versus j graph. This is shown in figure 17 for the case of negative non-classical shocks, where the result (4.6) expressed in terms of the original variables assumes the form

$$\left.\begin{gathered} \gamma > 0, \quad \hat{U}_b > -1 + \frac{4}{\sqrt{3}}\delta : \\ \hat{U} = \frac{\hat{U}_a + \hat{U}_b}{2} + \frac{[\hat{U}]}{2} \tanh \frac{|[\hat{U}]|\xi}{4\sqrt{3\gamma}}, \quad \hat{U}_a = -2 + \frac{2}{\sqrt{3}}\delta - \hat{U}_b. \end{gathered}\right\} \tag{4.8}$$

The fixed point relevant for the construction of positive non-classical shocks would be located above $\hat{U} = -1$. In the limit of vanishing dissipation, $\delta = 0$, both fixed points coincide with the inflexion point and one then obtains the result

$$\hat{U} = -1 - (1 + \hat{U}_b) \tanh \frac{|1 + \hat{U}_b|\xi}{2\sqrt{3\gamma}}, \quad \hat{U}_a = -2 - \hat{U}_b, \tag{4.9}$$

which is valid for positive as well as negative inviscid jumps. It is readily shown that this expression is equivalent to the inviscid-bore solutions of the modified Korteweg–de Vries equation, which have been known for some time and have been observed experimentally (e.g. Melville & Helfrich 1987; Baines 1995, pp. 128, 129). Apparently, however, their non-classical nature has not been recognized so far.

The above considerations indicate that the limiting form of the evolution equations (2.47) and (3.7) for non-dispersive non-dissipative waves is essentially incomplete and has to be supplemented with further information on how fast these effects tend to

https://doi.org/10.1017/S0022112006004071 Published online by Cambridge University Press

zero in this limit. According to the model adopted here, the appropriate solution of (3.7) is selected by the Oleinik admissibility criterion if the dispersion coefficient is negative or if dissipation is dominant. However, if dissipation is weak and if the effects of surface tension are sufficiently small that the dispersion coefficient is positive, the occurrence of non-classical shocks has to be taken into account.

It should be kept in mind, however, that for any solution of the shock-layer problem to describe the internal structure of an admissible hydraulic jump, its streamwise extent has to be so small that in the original variables $\hat{X}$ and τ of (4.1), the shock layer collapses into a jump discontinuity. If dissipation is dominant or a balance between dispersion and dissipation exists, i.e. $\alpha \gg \sqrt{|\gamma|}$ or $\alpha \sim \sqrt{|\gamma|}$, the shock-layer thickness is $O(\alpha)$ and, consequently, the above requirement is fulfilled as long as $\alpha \ll 1$. For $O(1)$ dissipation and small dispersion, jumps will obviously be heavily smeared even over ranges where the original scales are $O(1)$ quantities; however, this case is beyond the scope of the theory presented here. In the case of very weak dissipation, i.e. $\alpha \ll \sqrt{|\gamma|} \ll 1$, the situation turns out to be more complicated. If the jump is non-classical, its internal structure is characterized by downstream and upstream states that are both approached monotonically. Then the streamwise extent of the shock layer is $O(|\gamma|^{1/2})$, which again satisfies the requirement of an asymptotically thin shock layer. In contrast with that, a discontinuity having a shock-layer solution dominated by dispersion for which either the upstream state ($\gamma < 0$) or the downstream state ($\gamma > 0$) is approached in an oscillatory way (see figure 15) can then be regarded as an admissible classical jump only if the dissipation is still strong enough to ensure that the solution converges to a non-oscillatory upstream or downstream state within a inner spatial range that is much smaller than $O(1)$. Inspection of the problem (4.4) immediately shows that this requirement leads to the additional condition $\alpha \gg |\gamma|$. Some dissipation is obviously needed to guarantee the occurrence of classical jumps. The inviscid bore, therefore, represents the only possible solution in the limit of vanishing dissipation, $\delta = \alpha/\sqrt{\gamma} = 0$, $\gamma > 0$.

We conclude this section with an example which shows how such shocks influence steady flows over a bottom topography. Specifically, we return to a case investigated earlier: the flow past a single hump of the form described by (3.15) with $\sigma = 1$ having supercritical conditions far upstream; see figure 18. If $\gamma < 0$ or $\gamma > 0$ and $\delta \geqslant \sqrt{3}/2$, the Oleinik admissibility criterion holds and the resulting solutions contains two sonic hydraulic jumps, as pointed out before. Evaluation of (3.11) with $Q = 1$ shows that the positions of these jumps are given by $\hat{X} = -\operatorname{acosh}\sqrt{3} = -1.146$ and $\hat{X} = 0$, respectively. In the limit $\delta = \sqrt{3}/2$, the points $\hat{U} = 0$ and $\hat{U} = -2$ in figure 17, which characterize the sonic upstream and downstream states of these hydraulic jumps, are at the same time fixed points of Rayleigh lines associated with non-classical shocks, i.e. the two sonic hydraulic jumps can be interpreted also as non-classical hydraulic jumps of the minimum possible strength. If $\gamma > 0$ and δ decreases below the limiting value $\sqrt{3}/2$, these fixed points move closer to the inflexion point of the $\hat{U}$ versus j graph, thus generating solutions which contain non-classical hydraulic jumps that have larger amplitudes and are located further downstream. Finally, in the limit of lossless flow, $\delta = 0$, the two Rayleigh lines coincide and, as a consequence, the positions of the associated non-classical hydraulic jumps (inviscid bores), which now assume their maximum possible strength, are symmetrical with respect to $\hat{X} = 0$. For the example considered here, these jumps are located at $\hat{X} = \mp \operatorname{acosh}\sqrt{6}/2 = \mp 0.658$.

From the physical point of view, non-classical jumps are characterized by the fact that the wavefront leaves the discontinuity on one side, see figure 14(d), whereas if the dissipation is large enough that the Oleinik criterion (3.10) holds then the wavefronts

https://doi.org/10.1017/S0022112006004071 Published online by Cambridge University Press

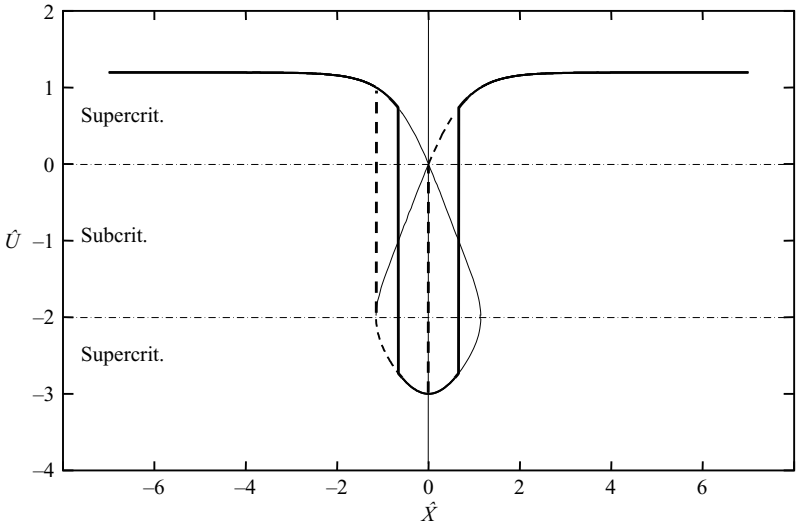


FIGURE 18. Steady solution with two inviscid bores (vertical solid lines) if $\delta = 0$; for $\delta \geqslant 3/2$ there are two viscosity-dominated sonic bores (vertical broken lines). $Q = 1$, $\sigma = 1$.

merge on the discontinuity from both sides or, as a limiting case, the waves leave it tangentially on one side (sonic jump); see figures 14(b) and 14(c). Exactly this difference in the two mechanisms determines which parts of the formally multivalued solutions of the wave equation (3.9) or, as in the case shown in figure 18, its steady counterpart (3.11) are realized. In other words, despite the fact that dispersive and viscous effects are small, the uniqueness of the 'hyperbolic' flow field governed by either (3.9) or (3.11) crucially depends on the ratio of dissipation and dispersion in the system, since both affect the inner shock structures. In order to demonstrate this phenomenon graphically, the different solutions for the characteristics $\xi = \text{constant}$ with $\mathrm{d}\hat{X}/\mathrm{d}\tau = v_w$ associated with the two steady distributions of $\hat{U}$ presented in figure 18, i.e. the classical case featuring two viscosity-dominated sonic bores and the non-classical case featuring two inviscid bores, are depicted in figures 19(a) and 19(b), respectively. In connection with the classical case, it should be noted that evaluation of $\mathrm{d}\tau/\mathrm{d}\hat{X} = 1/v_w$ together with the Oleinik condition (3.10) renders the slopes of the characteristics in the $(\hat{X}, \tau)$-plane, immediately after the first sonic jump, proportional to $\Delta\hat{X}^{-1/2}$, $\Delta\hat{X} \ll 1$. In contrast with this, the slopes after the second sonic jump turn out to satisfy the relationship $\mathrm{d}\tau/\mathrm{d}\hat{X} \propto \Delta\hat{X}^{-1}$, which leads to the conclusion that the wavefront is not able to leave the second jump in finite time. This result is a direct consequence of the fact that the flow is purely supercritical downstream of the hump but has a critical state at $\hat{X} = 0$, where $\mathrm{d}S/\mathrm{d}\hat{X} = 0$. It thus complements the discussion in § 3 (and see figure 11) concerning the stability of the supercritical continuous steady solution for $Q = 1$, where it was stated that the characteristics associated with the solution branch upstream of the hump cannot reach the crest in finite time. As shown in figure 19(b), a completely different picture emerges in the limit of lossless flow, $\delta = 0$, where the requirement of uniqueness of the solution leads to the formation of two inviscid bores. Since the Rayleigh lines associated with these non-classical shocks cut the $\hat{U}$ versus j graph at its inflection point $\hat{U} = -1$, the characteristic curves pass through the jumps without changing their slopes and reach the end of the flow domain under consideration within a finite period of time.

https://doi.org/10.1017/S0022112006004071 Published online by Cambridge University Press

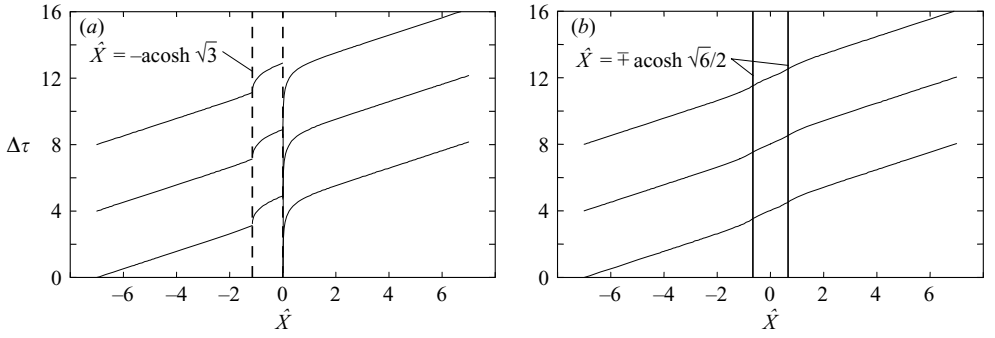


FIGURE 19. (*a*) Characteristic curves of the steady solution with two viscosity-dominated sonic bores, $\delta \geqslant \sqrt{3}/2$. (*b*) Characteristic curves of the steady solution with two inviscid bores, $\delta = 0$. $Q = 1$, $\sigma = 1$.

5. Conclusions

The main objective of this study is to provide insight into the effect of density stratification on the propagation of weakly nonlinear gravity waves in free-surface flows over a bottom topography when the unperturbed state is near critical. For simplicity a two-layer fluid model has been adopted and the liquids have been taken to be incompressible and inviscid. Furthermore, it has been assumed that the streamwise extent of the obstacle located on a horizontal flat bottom is large compared with the total depth of the flow, so that the fluid motion in both layers is governed by the one-dimensional form of the Euler equations with hydrostatic pressure distributions.

The analysis then shows that the two types of waves which have to be distinguished in a such a two-layer flow, i.e. the surface-layer waves and internal-layer waves, may exhibit remarkably different behaviour. In the first case, the resonant response to obstacle-forcing is governed by the inviscid Burgers equation with quadratic nonlinearity, which has been investigated in detail in the past and, therefore, has not been considered further here. The inviscid Burgers equation is found also to describe the evolution of internal-layer waves in general. However, there exists a finite range of the parameters characterizing the unperturbed state in which the quadratic nonlinear parameter is no longer of order unity but is of the same magnitude as the wave amplitude and even may change sign. An example is provided by flows whose unperturbed state is characterized by equal velocities and nearly equal fluid-layer thicknesses. As a consequence, internal-layer waves in this flow regime satisfy a modified inviscid Burgers equation which contains a cubic as well as a quadratic nonlinear term. This equation is known to arise also in studies dealing with weakly nonlinear acoustic waves in dense gases. Investigations carried out in this latter area over the past two decades have revealed a number of unexpected and unconventional properties associated with this equation. These include the occurrence of negative shocks, sonic shocks and split shocks.

The validity of the Oleinik criterion can be checked rigorously only by investigating the structure of the thin shock layer which emerges if physical effects such as internal friction, streamline curvature and surface tension, neglected in the purely hyperbolic approach, are accounted for. Unfortunately, however, complete formulations of the shock-layer problem associated with hydraulic jumps apparently do not exist at present. Even in the simplest case, that of laminar flow, so far only the initial phase of

https://doi.org/10.1017/S0022112006004071 Published online by Cambridge University Press

the flow development has been studied, which is not sufficient for the present purpose. In order to gain insight into how dissipative as well as dispersive mechanisms may affect the admissibility of jump discontinuities predicted by hyperbolic conservation laws, we have adopted the simplest model equation which reduces to the correct limit if viscosity plays an insignificant role compared with surface tension and streamline curvature. The general internal structure of hydraulic jumps is described then by travelling-wave solutions of this modified Burgers–Korteweg–de Vries equation (mBKdV), where dispersion and dissipation are balanced effects. It is found that the permissible jump discontinuities depend crucially on the precise ratio of dispersion and dissipation and, most importantly, may violate the Oleinik criterion, i.e. may emanate rather than absorb characteristics. Jump discontinuities having this unconventional property belong to the class of non-classical shocks, which has received increasing interest recently (Shearer 1988; LeFloch 1999; Kluwick *et al.* 2000). A prominent example is provided by the celebrated inviscid bore, which has been known for quite some time although its non-classical nature apparently has not been recognized so far.

As mentioned before, the mBKdV equation adopted here is asymptotically correct as far as dispersive effects are concerned. In other words, if lossless but (weakly) dispersive flow conditions are assumed then the model equation reduces to the asymptotically correct modified Korteweg–de Vries equation (mKdV) already discussed in the literature (see Melville & Helfrich 1987). In this case, the insertion of non-classical jumps, i.e. inviscid bores of vanishing shock-layer thickness, in order to remove regions of multivaluedness, turns out to be based completely on rational arguments. However, the mBKdV model provides only a very modest qualitative description of viscous effects and further progress in the evaluation of appropriate admissibility criteria required to complete existing hydraulic theories of one- and two-layer fluid flows will, therefore, strongly depend on the formulation of shock-layer equations which include both dispersion and dissipation in a rational manner. A first step in this direction was made recently by Kluwick, Exner & Cox (2000), who considered hydraulic jumps of small amplitude in single-layer fluids, assuming that viscous effects in the unperturbed flow are negligibly small except inside a thin laminar boundary layer adjacent to the solid boundary. Similarly to the studies by Gajjar & Smith (1983) and Bowles & Smith (1992), a structure comprising three layers or decks with different physical properties emerges in the large-Reynolds-number limit. Viscosity is found to affect the flow perturbations caused by a hydraulic jump inside a thin sublayer of the oncoming boundary layer, the so-called lower-deck region, only in leading order. Inside the rest of the boundary layer, the main-deck region, the flow perturbations are predominantly inviscid. They act to transfer the displacement effects exerted by the lower deck to a layer of inviscid fluid above the boundary layer, the upper-deck region, and to transfer the resulting pressure response to the lower-deck region thereby closing the flow description. In contrast with the studies by Gajjar & Smith (1983) and Bowles & Smith (1992), the triple-deck structure describes not only the initial departure from the unperturbed state but also the flow behaviour inside the whole shock layer. Furthermore, the pressure response in the outer, predominantly inviscid, region to the displacement resulting from the viscous-dominated wall layer is found to be nonlinear rather than linear, thus allowing for the passage through the critical state which occurs inside the shock layer. This analysis by Kluwick *et al.* (2000) has been extended to weakly nonlinear hydraulic jumps in two-layer fluids with quadratic nonlinearity, but work in progress indicates that a similar approach is possible also for two-layer fluids with mixed nonlinearity.

https://doi.org/10.1017/S0022112006004071 Published online by Cambridge University Press

REFERENCES

Adamson, T. C. Jr & Richey, G. K. 1973 Unsteady transonic flows with shock waves in two-dimensional channels. *J. Fluid Mech.* **60**, 363–382.

Akylas, T. R. 1984 On the excitation of long nonlinear water waves by a moving pressure disturbance. *J. Fluid Mech.* **141**, 455–466.

Armi, L. 1986 The hydraulics of two flowing layers with different densities. *J. Fluid Mech.* **163**, 27–58.

Baines, P. G. 1995 *Topographic Effects in Stratified Flows*. Cambridge University Press.

Bowles, R. I. & Smith, F. T. 1992 The standing hydraulic jump: theory, computations and comparison with experiments. *J. Fluid Mech.* **242**, 145–168.

Chu, V. H. & Baddour, R. E. 1977 Surges, waves and mixing in two-layer density stratified flow. *Proc. 17th Congr. Intl Assoc. Hydraul. Res.* **1**, 303–310.

Clarke, S. R. & Grimshaw, R. H. J. 1994 Resonantly generated internal waves in a contraction. *J. Fluid Mech.* **274**, 139–161.

Clarke, S. R. & Grimshaw, R. H. J. 1999 The effect of weak shear on finite-amplitude internal solitary waves. *J. Fluid Mech.* **395**, 125–159.

Clarke, S. R. & Grimshaw, R. H. J. 2000 Weakly nonlinear internal wave fronts trapped in contractions. *J. Fluid Mech.* **415**, 323–345.

Cole, S. L. 1985 Transient waves produced by flow past a bump. *Wave Motion* **7**, 579–587.

Cramer, M. S. & Crickenberger, A. B. 1991 The dissipative structure of shock waves in dense gases. *J. Fluid Mech.* **223**, 325–355.

Cramer, M. S. & Kluwick, A. 1984 On the propagation of waves exhibiting both positive and negative nonlinearity. *J. Fluid Mech.* **142**, 9–37.

Cramer, M. S. & Sen, R. 1992 General scheme for the derivation of evolution equations describing mixed nonlinearity. *Wave Motion* **15**, 333–355.

Gajjar, J. S. B. & Smith, F. T. 1983 On hypersonic self-induced separation, hydraulic jumps and boundary layers with algebraic growth. *Mathematica* **30**, 77–91.

Germain, P. 1972 Shock waves, jump relations and structure. *Adv. Appl. Mech.* **12**, 131–184.

Grimshaw, R., Pelinovsky, E. & Talipova, T. 1997 The modified Korteweg-de Vries equation in the theory of large-amplitude internal waves. *Nonl. Processes Geophys.* **4**, 237–250.

Grimshaw, R. H. J. & Smyth, N. 1986 Resonant flow of a stratified fluid over topography. *J. Fluid Mech.* **169**, 429–464.

Gustafsson, B. & Sundstrom, A. 1978 Incompletely parabolic problems in fluid dynamics. *SIAM J. Appl. Maths* **35**, 343–357.

Hayes, B. T. & LeFloch, P. G. 1997 Non-classical shocks and kinetic relations: scalar conservation laws. *Arch. Rat. Mech. Anal.* **139**, 1–56.

Helfrich, K. R., Melville, W. K. & Miles, J. W. 1984 On interfacial waves over slowly varying topography. *J. Fluid Mech.* **149**, 305–317.

Jacobs, D., McKinney, B. & Shearer, M. 1995 Travelling wave solutions of the modified Korteweg-de Vries Burgers equation. *J. Diffl Equat.* **116**, 448–467.

Jiang, Q. & Smith, R. B. 2001*a* Ideal shocks in two layer flow. Part I: Under a rigid lid. *Tellus* **53A**, 129–145.

Jiang, Q. & Smith, R. B. 2001*b* Ideal shocks in two layer flow. Part II: Under a passive layer. *Tellus* **53A**, 146–167.

Kakutani, T. & Yamasaki, N. 1978 Solitary waves on a two-layer fluid. *J. Phys. Soc. Japan* **45**, 674–679.

Keyfitz, B. L. 1995 A geometric theory of conservation laws which change type. *Z. Angew. Math. Mech.* **75**, 571–581.

Kluwick, A. 1972 Schallnahe Wellenausbreitungsvorgänge in schlanken Düsen. *Acta Mech.* **15**, 105–119.

Kluwick, A. 1991*a* Small-amplitude finite-rate waves in fluids having both positive and negative nonlinearity. In *Nonlinear Waves in Real Fluids* (ed. A. Kluwick). CISM Courses and Lectures, vol. 315, pp. 1–43. Springer.

Kluwick, A. 1991*b* Weakly nonlinear kinematic waves in suspensions of particles in fluids. *Acta Mech.* **88**, 205–217.

Kluwick, A. 1993 Transonic nozzle flow of dense gases. *J. Fluid Mech.* **247**, 661–688.

https://doi.org/10.1017/S0022112006004071 Published online by Cambridge University Press

Kluwick, A. 2001 Rarefaction Shocks. In *Handbook of Shock Waves* (ed. G. Ben-Dor, T. Elprin & O. Igra), pp. 339–411. Academic.

Kluwick, A. & Cox, E. A. 1998 Nonlinear waves in materials with mixed nonlinearity. *Wave Motion* **27**, 23–41.

Kluwick, A., Cox, E. A. & Scheichl, St. 2000 Non-classical kinematic shocks in suspensions of particles in fluids. *Acta Mech.* **144**, 197–210.

Kluwick, A. & Czemetschka, E. 1990 Kugel- und Zylinderwellen in Medien mit positiver und negativer Nichtlinearität. *Z. Angew. Math. Mech.* **70**, T207–208.

Kluwick, A., Exner, A. & Cox, E. A. 2000 Strucuture of small amplitude hydraulic jumps in laminar high Reynolds number flow. *Paper Presented at the 4th Euromech Fluid Mechanics Conference, Eindhoven, Nov 19-23, 2000.*

Kluwick, A. & Scheichl, St. 1996 Unsteady transonic nozzle flow of dense gases. *J. Fluid Mech.* **310**, 113–137.

Lax, P. D. 1957 Hyperbolic systems of conservation laws II. *Comm. Pure Appl. Maths* **10**, 537–566.

LeFloch, Ph. G. 1999 An introduction to nonclassical shocks of systems of conservation laws. In *An Introduction to Recent Developments in Theory and Numerics for Conservation Laws* (ed. D. Kröner, M. Ohlberger & C. Rohde), pp. 28–72. Springer.

LeVeque, R. J. 1992 *Numerical Methods for Conservation Laws*. Birkhäuser.

Lighthill, J. 1978 *Waves in Fluids*. Cambridge University Press.

Lowe, R. J., Rottman, J. W. & Linden, P. F. 2005 The non-Boussinesq lock-exchange problem. Part 1. Theory and experiments. *J. Fluid Mech.* **537**, 101–124.

Melville, W. K. & Helfrich, K. R. 1987 Transcritical two-layer flow over topography. *J. Fluid Mech.* **178**, 31–52.

Oleinik, O. 1959 Uniqueness and stability af the generalized solution of the cauchy problem for a quasi-linear equation. *Usp. Math. Nauk* **14**, 165–170.

Oleinik, O. 1964 Uniqueness and stability af the generalized solution of the cauchy problem for a quasi-linear equation. *Am. Math. Soc. Transl. Ser.* **33**, 285–290.

Peregrine, D. H. 1974 Water-wave interaction in the surf zone. *Proc. 14th Coastal Engng Conf.*, vol. 1, pp. 500–517.

Schär, C. & Smith, R. B. 1993 Shallow-water flow past an isolated topography. Part I: Vorticity production and wake formation. *J. Atmos. Sci.* **50**, 1373–1400.

Shearer, M. 1988 Dynamic phase transitions in a van der Waals gas. *Q. J. Appl. Maths* **46**, 631–636.

Shen, S. 1992 Forced solitary waves and hydraulic falls in two-layer flows. *J. Fluid Mech.* **234**, 583–612.

Smith, R. B. & Smith, D. F. 1995 Pseudoviscid wake formation by mountains in shallow water flow with a drifting vortex. *J. Atmos. Sci.* **52**, 436–454.

Stastna, M. & Peltier, W. R. 2005 On the resonant generation of large-amplitude internal solitary and solitary-like waves. *J. Fluid Mech.* **543**, 267–292.

Thompson, P. A. 1971 A fundamental derivative in gasdynamics. *Phys. Fluids* **14**, 1843–1849.

Whitham, G. B. 1974 *Linear and Nonlinear Waves*. John Wiley & Sons.

Wood, I. R. & Simpson, J. E. 1984 Jumps in layered miscible fluids. *J. Fluid Mech.* **140**, 329–342.

Yih, C. S. & Guha, C. R. 1955 Hydraulic jump in a fluid system of two layers. *Tellus* **7**, 358–366.

https://doi.org/10.1017/S0022112006004071 Published online by Cambridge University Press